Experimental assessment of ground-truth faults in a typical single-duct dual-fan air-handling unit under Mediterranean climatic conditions: Impact scenarios of sensors? offset

Experimental assessment of ground-truth faults in a typical single-duct dual-fan air-handling unit under Mediterranean climatic conditions: impact scenarios of sensors' offset and fans' failure

Antonio Rosato[1,*], Francesco Guarino[1], Mohammad El Youssef[1], Alfonso Capozzoli[2], Massimiliano Masullo[1], Luigi Maffei[1]

[1] Department of Architecture and Industrial Design, University of Campania Luigi Vanvitelli, Via San Lorenzo 4, 81031 - Aversa, Italy
[2] Department of Energy "Galileo Ferraris", Politecnico di Torino, Corso Duca degli Abruzzi 24, 10129 Turin, Italy
*Corresponding author

Abstract
Data-driven Automated Fault Detection and Diagnosis (AFDD) is the automated process of detecting deviations (faults) from normal operation and diagnosing the type of problem and/or its location based on the exploitation of data collected under normal and faulty conditions. The performance of a typical single-duct dual-fan constant air volume air-handling unit (AHU) are investigated through a number of experiments performed during Italian cooling and heating seasons under both fault free and faulty scenarios. The AHU operation is analysed while artificially introducing six typical faults: 1) positive offset (+3 °C) of the return air temperature sensor; 2) negative offset (–3 °C) of the return air temperature sensor; 3) positive offset (+15%) of the return air relative humidity sensor; 4) negative offset (–15%) of the return air relative humidity sensor; 5) complete failure of the return air fan; 6) complete failure of the supply air fan. The faulty tests are compared with the fault free experiments performed under the same boundary conditions to assess the impacts of the faults on both thermal/hygrometric indoor comfort and patterns of key operating parameters with the aim of supporting the studies focusing on new and accurate data-driven AFDD methods for AHUs.

Keywords: Air-handling unit, fan failure, sensor offset, experimental faulty data, fault impact scenario, fault detection and diagnosis, energy management and efficiency.

1. Introduction

In 2020 the building sector was responsible for about 36% of global final energy use and around 37% of worldwide energy-related greenhouse gas (GHG) emissions [1]. Heating, Ventilation and Air-Conditioning (HVAC) systems are used to control indoor air temperature, indoor air relative humidity, indoor air velocity and indoor air quality inside buildings. The most common HVAC systems include Air-Handling Units (AHUs) consisting of a significant number of interconnected components (coils, fans, valves, dampers, actuators, filters, etc.) and measuring sensors at risk of failure, which may affect end-user comfort, energy efficiency, GHG emissions, operational/maintenance costs and equipment lifetime. According to several scientific studies [2-4], HVAC systems are in charge of roughly 50÷60% of the energy demand of the building sector and 10÷20% of the overall energy consumption. With reference to this point, in the scientific literature it is clearly highlighted that: (i) HVAC systems are frequently operated in faulty conditions due to lack of proper maintenance, components' failure or incorrect installation; (ii) faulty operation greatly affects the performance of HVAC units. In more detail, a survey in California (U.S.A.) highlighted that 65% of residential cooling systems and 71% of commercial cooling systems are characterized by faulty operation [4]. Proctor [5] reported that about 90% of more than 55,000 AHUs operating in U.S.A. runs with one or multiple faults. Furthermore, Rossi [6] found an average operating efficiency of 1468 roof top units equal to about 80% of the designed performance. In a study focusing on buildings located in U.K., the results showed that around 25÷50% of energy is wasted due to faults of HVAC systems [7]. Yun et al. [4] also indicated that faulty operation of HVAC systems can cause an increase of approximately 5÷30% in terms of energy demand; other scientific researches [8,9] showed that an energy saving of 20÷30% can be achieved by recommissioning HVAC systems to rectify faulty operation. Finally, Deshmukh et al. [10] estimated that faulty operation of HVAC systems is responsible for about 20% of the energy consumption of buildings.

Companies generally adopt two different types of maintenance (reactive or preventive) to guarantee the reliability of HVAC systems [11,12]. In the case of reactive maintenance, the repairs are performed only after the component failure. This kind of approach could (i) be extremely expensive and (ii) cause safety issues. In the case of preventive maintenance, the systems are inspected and maintained at pre-set time intervals; however, the maintenance interval is difficult to be defined taking into account that it must be conservative to prevent safety issues and reduce fault costs, but scheduling the maintenance very early could mean wasting system life that is still usable. The above-mentioned critical points associated with both reactive and preventive maintenance programs could be strongly limited thanks to the Automated Fault Detection and Diagnosis (AFDD), that is defined as an automated process of detecting deviations (faults) from the normal or expected operation and diagnosing the type of problem and/or its location [3,4,7]. According to [3,4,7], AFDD strategies represent one of the most active areas of research as well as a very fast-growing market segment in the context of building analytics technologies. In particular, two International Energy Agency (IEA) Annex reports [13,14] and several literature reviews [3,7,15] are available with reference to this research field, certifying the relevance of this topic. Several studies [3,7,14] indicated that AFDD technologies can offer several interrelated benefits for equipment owners, including energy savings, operating cost reduction, lower GHG emissions, improved indoor comfort as well as longer lifetime. Service contractors can also benefit from increased efficiency and reduced costs; manufacturers benefit from warranty cost savings; owners of AFDD tools can benefit from the majority of the service cost savings; at a higher level, society can benefit from better environmental protection, energy savings, emission reductions and more consistent service distribution. Yu et al. [7] underlined that an effective identification and diagnosis of the faults in AHUs could save from 15% up to 30% of the total energy consumed by buildings. Au-Yong et al. [16] also highlighted the importance of AFDD methods, suggesting several maintenance factors to be correlated with the satisfaction of occupants. Frank et al. [17] suggested that a widespread adoption of AFDD algorithms would deliver an estimated 5%÷15% energy saving with reference to the sector of commercial buildings.

The methods used for performing AFDD analyses can be classified in: (i) quantitative model-based, (ii) qualitative model-based and (iii) data driven-based [3,7,17]. In comparison to quantitative model-based and qualitative model-based methods, the data driven-based approach is easier to be utilized mainly thanks to (i) the development of various computer-aided techniques, (ii) the low-cost installation of sensors as well as (iii) the possibility to be also applied when the physics-based knowledge is not wide enough [3,7,18]. The category of data driven-based AFDD tools includes methodologies based on the exploitation of data collected under normal and faulty conditions allowing for the detection of faults by analysing the changes of selected variable patterns and searching the causes according to similarities with pre-labelled anomaly libraries [3,7,18]. An effective assessment of the effects associated with fault occurrence is, therefore, critical to the development of an effective fault prioritization and data driven-based AFDD algorithms.

1.1 Research gaps

Although data-driven AFDD methods could represent a powerful approach to ensuring more efficient operations of AHUs and related technology is maturing, they are still in the relatively early stage of adoption stock-wide [19]. A significant debate continues and uncertainties remain regarding the accuracy and effectiveness of both research-grade and commercial AFDD products (also because there is not yet a generally accepted standard for evaluating the performance of AFDD algorithms [17,18]) and several research gaps are still to be addressed.

In particular, the adoption of data-driven AFDD models for AHUs requires labelled, reliable, affordable, and scalable experimental data that are difficult to be obtained and still limited due to the facts that [3,7,20]: (i) AHUs are non-stationary systems because they operate under varying weather/load conditions; (ii) the architecture of sensors network in AHUs is usually not designed for AFDD purposes and, therefore, some important parameters are not measured; (iii) measurements under faulty conditions are challenging to be obtained due to the inconvenience of implementing faults into complex and expensive devices with the purpose of collecting data; (iv) high-level domain expertise and manual inspections are generally required for data labelling, making it expensive and time-consuming for practical applications; (v) different faults may have similar symptoms and, therefore, high accuracy sensors have to be used for measuring the required parameters; (vi) the simultaneous occurrence of multiple faults should be investigated, but interaction of faults is usually synergistic and makes difficult to isolate the effects of each single fault; (vii) weather and heating/cooling loads can significantly affect the fault symptoms and data-driven AFDD tools generally cannot extrapolate beyond the range of training data (thus, huge experimental campaigns exploring wide ranges of operating conditions have to be carried out).

The most part of the experimental datasets for AFDD of AHUs have been mainly developed with reference to American weather conditions [21-23], with a very few examples of measurements taken under Italian climates [24-26]. In addition, it should be underlined that the sampling frequency of measurements represents an important parameter to be selected in order to accurately characterize both transient and steady-state operation of AHU components; a minimum measurement frequency of 35 s [27,28] has been considered in the experimental studies focusing on the development of AFDD strategies for AHUs, but most of them used 1 minute as sampling rate [20,22,26]. Several data-driven AFDD methods have been developed based on the ASHRAE RP-1312 dataset [20], that is dated 2011; it has been created by means of a simulation model developed via the HVACSIM+ software [29] and then validated using measured data (recorded at 1-minute intervals during both fault free and faulty operation under summer and winter conditions) from an experimental set-up consisting of two identical HVAC systems including variable air volume (VAV) AHUs (one operating under fault free conditions and the other one running under faulty conditions with manually implemented faults). As a consequence, even if several scientific works focusing on data-driven AFDD methods have been developed, the scientific literature [3,7,19] highlights that faulty datasets to support the adoption of data-driven AFDD methods are limited and they refer to reduced ranges of weather/load conditions and fault types/severities.

Experimental faulty datasets of AHUs are also fundamental not only for developing new AFDD tools, but also as reference ground to benchmark the performance across AFDD algorithms. To the knowledge of the authors, only 5 out of these datasets with verified ground truth information on specific tagged faults are currently publicly available [22]. Lin et al. [19] underlined that there is a lack of datasets for assessing the accuracy of AFDD tools and additional works should be performed in order to provide further public databases, together with a clear characterization of fault categories. Granderson et al. [21] also highlighted a growing need for AHU faulty datasets that can be utilized to further evaluate the accuracy of AFDD methods. More recently, Granderson et al. [22] indicated that it is rare to find databases characterized by ground-truth verified points together with a clear indication of operating states they represent (healthy, faulty, or simply unusual). In addition, Casillas et al. [30] noticed that one of the most significant challenges of researches regarding AFDD methods is represented by the insufficient availability of shared datasets to compare the performance of AFDD algorithms with the aim of prioritizing related future investments. Finally, Hu et al. [31] underlined that other research is required to obtain more public experimental data under both normal and faulty operation of HVAC units (while considering the occurrence of a number of different faults) upon varying the boundary conditions for developing and assessing new accurate data-driven AFDD tools.

Furthermore, it should be highlighted that a few studies quantitatively examined how various fault types and severities can impact on users' comfort, patterns of key parameters, energy consumption, GHG emissions, operating and maintenance cost and equipment life cycle based on empirical field data [17,19,21]; with respect to this point, additional efforts could be fundamental in guiding the future development of AFDD technologies. Chen et al. [32] highlighted that, in the research field of HVAC systems, most of the scientific studies investigated the fault effects in terms of annual energy consumption or costs or indoor comfort, but little research has been performed in order to quantitatively assess the fault effects on various measurements, which are increasingly used to monitor and control equipment operation, assess system dynamic operation as well as develop data-driven AFDD tools.

The exploitation of simulated datasets could represent an alternative to the collection of experimental measurements through AHU digital twins/models which can make easier the generation of faulty data under broader faulty operational scenarios [33-35]. However, they must be experimentally validated to avoid that the extracted knowledge does not reflect the real behaviour of the system and, according to the scientific literature [36], only one detailed AHU digital twin validated against measured data is publicly available [20].

Finally, the scientific literature related to AFDD tools indicates that several components of HVAC systems often fail during day-to-day operation. According to [21], sensors, actuators and fans are the most common elements of AHUs that fail or give erroneous signals. Li and O'Neill [34] highlighted that the fan is one of the most critical components of AHUs and the associated common faults include burn-out motor, loosed or broken belt, out of balance impeller, power control issues, etc.; they [34] also underlined that it is common for the sensors to have offsets that are typically random (either extra positive or extra negative values adding to the normal readings can be recognized). Montazeri and Kargar [37] indicated that actuator and sensor faults are inevitable in AHUs and highlighted that the supply air fan stuck is one of the most frequent faults occurring in AHUs. Cho et al. [38] underlined that sensors, actuators and fans are the most common elements that fail or give erroneous signals among the components of HVAC systems. Dey et al. [39] assessed the occurrence probability of 14 fault types associated to heating coil, cooling coil, outside air mixing box, controller and

sensors based on one-year maintenance records related to a VAV AHU serving the Applied Engineering and Technology building at the University of Texas (San Antonio, U.S.A.); the data indicated that the heating coil valve leaking and the return air dumper stuck are the most frequent fault types (with an occurrence probability of 10.9%), while the return air temperature biased, the supply air temperature biased and the mixing air temperature biased are characterized by an occurrence probability equal to 8.7%. In the IEA Annex 34 [14] it is also indicated that sensors are often faulty and frequently result in incorrect measurements, especially sensors used to measure parameters associated with the air in a zone or duct. To the knowledge of the authors, the offset of the return/indoor air temperature sensor has been experimentally investigated only in four scientific studies. In particular, Granderson et al. [22] explored the operation of a VAV AHU in the case of positive (+2.2 °C) and negative (–2.2 °C) offset of the indoor air temperature sensor by means of daily tests (with a frequency of measurements equal to 1 minute) performed during winter under the climatic conditions of Iowa and Tennessee (U.S.A.); the authors provided detailed information about the dataset (with particular reference to the fault severity as well as the experimental set-up), but they did not explained the impacts associated to the occurrence of the faults. Liu et al. [23] examined a positive offset of 3 °C associated to the measures provided by the return air temperature sensor during summer, winter and fall seasons of Iowa (U.S.A.) by means of 3 testing days (data collected at 1-minute sampling rate) with reference to a VAV AHU; the authors found that this fault does not adversely affect the system performance during all three investigated seasons. Cho et al. [38,40] analysed the effects of positive offsets (+10% and 20%) associated with the measurements of indoor air temperature with reference to the operation of a VAV AHU only during winter by means of 90-min experiments; they found that (i) a significant effect on the VAV AHU damper opening can be recognized and (ii) it takes about 50÷60 minutes to get again the steady-state operation. Faults associated with the supply and return air fans have been considered only in 4 scientific papers. In particular, in [20] a supply air fan failure as well as a return air fan stuck (at 20%, 30% and 80% as level of severity) have been investigated during winter, spring and summer of Iowa (U.S.A.), with reference to the experimental operation of a VAV AHU (data recorded at 1-min intervals), but the effects corresponding to the investigated faults have not been analyzed. Liu et al. [23] analysed both the return air fan failure (during fall only) and the supply air fan failure (during both summer and winter) in the case of a VAV AHU serving 4 test rooms and operating in Iowa (U.S.A.) by means of daily experimental tests (with data collected at 1-minute sampling rate). The experiments indicated that (i) the cooling supply air fan failure causes overheating in the test rooms, (ii) the heating supply air fan failure causes both 100% opening of the hot deck VAV damper and overcooling of the test rooms, (iii) the return air fan failure results in high pressurization of the test rooms. Feng et al. [41] studied the performance of an innovative AFDD method in the case of both the return air fan failure and the return air fan stuck at 30% only during the summer operation of a VAV AHU located in Hefei (China) through experiments of 10 hours (with data collected every 5 minutes); the analysis demonstrated that the proposed tool is characterized by improved results with respect to other methods available in the literature, but additional efforts have to be performed in order to make possible its application to wider operating scenarios. Finally, Nehasil et al. [42] experimentally validated the accuracy of a new tool for the detection of both the return air fan and the supply air fan failures on the performance of a CAV AHU operating in Bustehrad (Czech Republic); a 90% detection rate of the developed method has been demonstrated in the study. The above literature review clearly highlights that the studies related to sensors' offset and fans' failure (i) are limited in number, (ii) have not been performed under Mediterranean climatic conditions, (iii) in some cases have been conducted only during a single season, (iv) have been carried out with a sampling rate of experimental data not lower than 1 minute; therefore, it can be underlined that additional experimental researches focusing on both offsets of return/indoor air temperature/humidity sensors and failure of fans are required.

1.2 Novelty, goals and structure of the paper

This paper addresses some of the above-mentioned most critical barriers limiting the application of data-driven AFDD tools for AHUs mainly thanks to the development of a newly curated dataset with known ground-truth conditions and high-quality data representing both fault free and controlled faulty operating conditions of the typical HVAC system including a single-duct dual-fan constant air volume AHU of the SENS i-Lab of the Department of Architecture and Industrial Design of the University of Campania Luigi Vanvitelli (Aversa, south of Italy) [43]. The system includes (i) a network of accurate sensors able to fully monitor and record its operation upon varying the boundary conditions, as well as (ii) a specifically-devoted control system allowing to artificially implement selected faults of the main system components and sensors. The experimental data have been recorded during both Italian summer and winter at 1-second intervals by performing daily tests with a continuous duration of 9 hours, thus allowing to accurately characterize both transient and steady-state

behaviour of the AHU. In particular, the operation of the AHU has been analysed while artificially introducing the following 6 different typical faults:

1) positive offset of the return air temperature sensor (+3 °C);
2) negative offset of the return air temperature sensor (–3 °C);
3) positive offset of the return air relative humidity sensor (+15%);
4) negative offset of the return air relative humidity sensor (–15%);
5) complete failure of the return air fan;
6) complete failure of the supply air fan.

In this study, the measured faulty data have been also compared with the experimental tests performed without faults (assumed as baselines) under the same boundary conditions. This comparison has been carried out in order to quantitatively assess the impacts of the selected faults on thermal and hygrometric indoor comfort conditions as well as patterns of key operating parameters.

The main aims of this study can be summarized as follows:

- collecting high-resolution faulty performance data of a typical AHU covering different fault types/severities over a wide range of Italian operating conditions to be publicly delivered in order to (i) help building operators and facility engineers in recognizing different fault patterns and identifying faults of AHUs, (ii) support the development of, and benchmark the performance accuracy of FDD methods, (iii) develop AHU digital twins with the aim of generating new faulty operational datasets covering broader operating scenarios, (iv) facilitate the future development of new and accurate AFDD for typical AHUs, (v) understand how AFDD technology overall is improving over time;
- assessing the gap between AHU faulty operation and design expectations;
- performing fault impact scenario analyses based on the experimental data in order to assess the effects associated with the occurrence of typical AHU fault types/severities in terms of thermo-hygrometric indoor comfort conditions and patterns of key operating parameters;
- identifying the most impacted key-operating parameters by evaluating the symptoms occurrence probability;
- helping in selecting the threshold tolerance values required by data-driven rule-based AFDD methods.

In more detail, the paper consists of six main sections. Section 2 describes the experimental setup together with related sensors and control logics. Section 3 paints a picture of the experimental fault free and faulty tests, detailing the characteristics of the implemented faults. Boundary conditions of the fault free and faulty experiments are compared in Section 4. An assessment of faults' impact in terms of users' comfort and patterns of key parameters is performed and discussed in Sections 5 (and related subsections 5.1 and 5.2). Finally, the conclusions and future research steps are reported in Section 6.

2. Description of the experimental set-up

The SENS i-Lab is an innovative, multi-sensorial and multi-purpose laboratory of the Department of Architecture and Industrial Design of the University of Campania Luigi Vanvitelli (Aversa, south of Italy, latitude: 40°58'21" N, longitude: 14°12'26" E) [43]. It consists of an integrated test room housed in the department itself and characterized by a floor area of 16.0 m^2, a height of 3.6 m, four vertical walls (with one door, but without windows), a horizontal ceiling as well as a horizontal floor. Table 1 describes the main characteristics of layers composing the envelope of the integrated test room.

Table 1. Integrated test room envelope's characteristics.

Element of the integrated test room	Layer material (from outside to inside)	Thickness (m)	Thermal conductivity (W/mK)	Conductive thermal resistance (m^2K/W)		Area (m^2)
Horizontal ceiling	Plasterboard	0.0125	0.250	0.050	2.023	16.00
	Rock wool	0.0800	0.042	1.905		
	Polyurethane panel	0.0150	0.220	0.068		
Horizontal floor	Subfloor	0.1000	1.350	0.074	3.107	16.00
	Tiles	0.0500	2.100	0.024		
	Polystyrene panel	0.0800	0.035	2.286		
	Galvanized steel slab	0.0020	52.000	0.000		
	Tiles	0.0100	1.050	0.010		
West- and East-oriented vertical walls	Plasterboard	0.0125	0.250	0.050	1.955	14.40
	Rock wool	0.0800	0.042	1.905		
South- and North-oriented vertical walls	Plasterboard	0.0125	0.250	0.050	1.998	14.4
	Rock wool	0.0800	0.042	1.905		
	Fibre-cement panel	0.0150	0.350	0.043		
Door (South-oriented)	Soft wood	0.0500	0.140	0.357	0.357	1.68

The integrated test room is served by a typical HVAC system, including a single-duct dual-fan constant air volume AHU, capable to control air temperature, air relative humidity, air velocity and air quality inside the room. Figure 1 reports the schematic of the AHU including the following main functional components: return air fan (RAF); supply air fan (SAF); pre-heating coil (PreHC); post-heating coil (PostHC); cooling coil (CC); steam humidifier (HUM); static cross-flow heat recovery system (HRS); vapor compression air-to-water electric refrigerating system (RS) connected with the cooling coil via a 75 liter cold tank (CT); vapor-compression air-to-water electric heat pump (HP) connected with both the pre-heating coil and the post-heating coil via a 75 liter hot tank (HT); four valves (V_{PreHC}, V_{PostHC}, V_{CC}, V_{HUM}) controlling the flow rate of the heat carrier fluid entering, respectively, the pre-heating coil, the post-heating coil, the cooling coil and the steam humidifier; return air damper (D_{RA}); outside air damper (D_{OA}); exhaust air damper (D_{EA}); damper of the HRS (D_{HRS}); return air filter (RAFil); outside air filter (OAFil); supply air filter (SAFil); ducts to transfer the air to (SAD) and from (RAD) the conditioned space. The heat carrier fluid is a mixture of water and ethylene glycol (6% by volume). Two 0.08×0.18 cm^2 air grilles are mounted on the south-oriented wall at floor level and two 0.08×0.18 cm^2 air grilles are mounted on the north-oriented wall at floor level with the aim of extracting air from the indoor space to be moved into the AHU; a 0.60×0.60 cm^2 swirl diffuser is mounted in the centre of the ceiling of the test room. A view of the external part of the AHU serving the test room of the SENS i-Lab is reported in Figure 2.

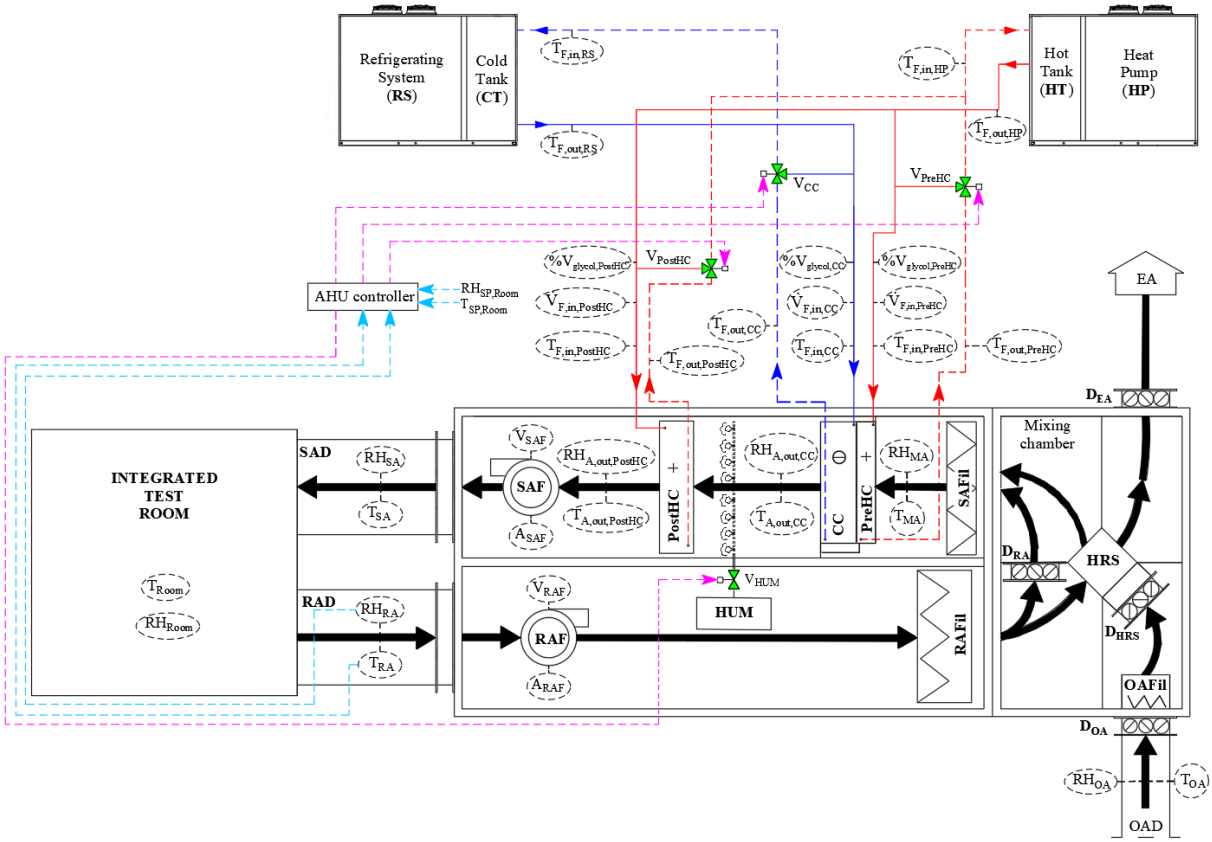

Figure 1. Schematic of the AHU of the SENS i-Lab.

Figure 2. External view of the AHU of the SENS i-Lab.

Table 2 reports the most important characteristics of the main components of the AHU.

Table 2. Characteristics of the main AHU components.

Supply (SAF) air fan	Nominal supply air flow rate (m^3/h)	600
	Nominal power (kW)	2.50
Return (RAF) air fan	Nominal return air flow rate (m^3/h)	600
	Nominal power (kW)	0.50
	Nominal efficiency (%)	74.7

Cross flow heat recovery system (HRS)	Recovery capacity (kW)	3.1
Pre-heating coil (PreHC)	Nominal heating capacity (kW)	4.1
	Nominal heat carrier fluid flow rate (m^3/h)	0.71
	Nominal air flow rate (m^3/h)	600
Cooling coil (CC)	Nominal cooling capacity (kW)	5.0
	Nominal heat carrier fluid flow rate (m^3/h)	0.86
	Nominal air flow rate (m^3/h)	600
Humidifier (HUM) [44]	Nominal steam capacity (kg/h)	5.0
	Nominal power (kW)	3.7
Post-heating coil (PostHC)	Nominal heating capacity (kW)	5.0
	Nominal heat carrier fluid flow rate (m^3/h)	0.86
	Nominal air flow rate (m^3/h)	600
Heat pump (HP) [45]	Nominal heating capacity (kW)	13.8
	Nominal input power (compressor + fans) (kW)	4.5
Refrigerating system (RS) [45]	Nominal cooling capacity (kW)	13.6
	Nominal input power (compressor + fans) (kW)	4.2

According to the manufacturer data [45], the performance maps of the heat pump and the refrigeration unit are reported in Figure 3a and Figure 3b indicating, respectively, the coefficient of performance COP of the heap pump (useful thermal power output divided by required electric power input) and the energy efficiency ratio EER of the refrigerating system (useful cooling power out-put divided by required electric power input) as a function of supply fluid temperature and outside air temperature. The values of COP for the HP range from 2.2 up to 10.1, while the values of EER for the RS are in the range 2.3÷11.7.

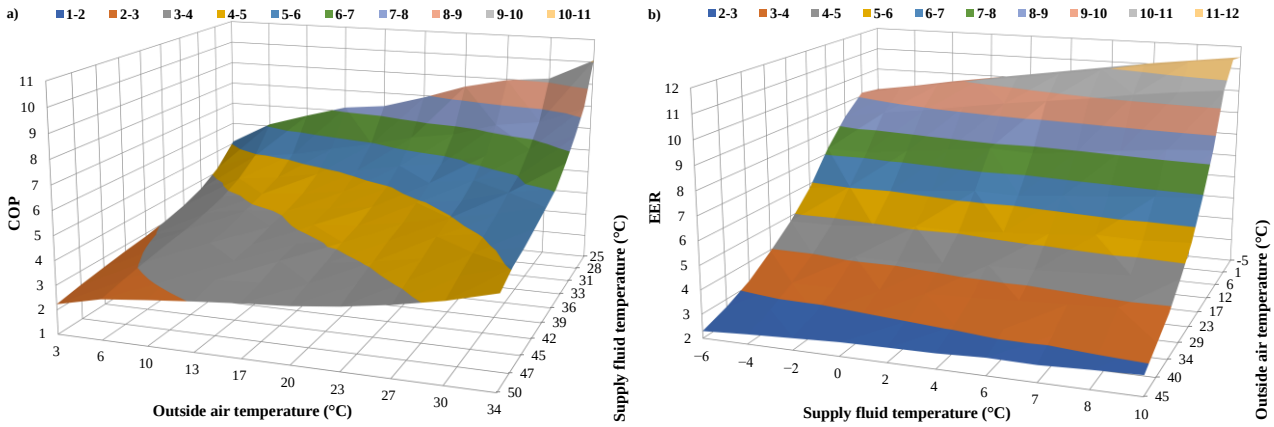

Figure 3. (a) COP of the HP and (b) EER of the RS upon varying outside air temperature and supply fluid temperature [45].

2.1 Sensors and measurement uncertainty

The AHU is fully equipped in order to monitor, control and record the key parameters of the HVAC system. The accuracy of measurements has to be indicated in order to quantify the reliability of test data [46]. The main characteristics of the sensors (measuring range and accuracy) are reported in Table 3. The measurement points are representative of points commonly monitored in building control systems. The supply and return air temperature/relative humidity sensors are inserted in the appropriate ducts.

Table 3. Characteristics of the AHU sensors.

Measured parameter	Measuring range	Accuracy
Return air temperature T_{RA}, Supply air temperature T_{SA}, Mixed air temperature T_{MA}, Cooling coil outlet air temperature $T_{A,out,CC}$ [47]	0 ÷ 50 °C	±0.80 °C
Post-heating coil outlet air temperature $T_{A,out,PostHC}$ [47]	−40 ÷ 60 °C	±0.80 °C
Outside air temperature T_{OA} [48]	−40 ÷ 60 °C	from −40 °C to 20 °C: $(-0.0083 \cdot T_{OA} + 0.3667)$ °C; from 20 °C to 60 °C: $(0.0088 \cdot T_{OA} + 0.025)$ °C
Air temperature inside the integrated test room T_{Room} [49]	−10 ÷ 60 °C	±0.50 °C
Pre-heating coil outlet heat carrier fluid temperature $T_{F,out,PreHC}$, Pre-heating coil inlet heat carrier fluid temperature $T_{F,in,PreHC}$, Post-heating coil outlet heat carrier fluid temperature $T_{F,out,PostHC}$, Post-heating coil inlet heat carrier fluid temperature $T_{F,in,PostHC}$, Cooling coil outlet heat carrier fluid temperature $T_{F,out,CC}$, Cooling coil inlet heat carrier fluid temperature $T_{F,in,CC}$ [50]	−10 ÷ 120 °C	±0.10 °C
Heat pump outlet heat carrier fluid temperature $T_{F,out,HP}$, Heat pump inlet heat carrier fluid temperature $T_{F,in,HP}$, Refrigerating system outlet heat carrier fluid temperature $T_{F,out,RS}$, Refrigerating system inlet heat carrier fluid temperature $T_{F,in,RS}$ [50]	−10 ÷ 60 °C	±0.03 °C
Return air relative humidity RH_{RA}, Supply air relative humidity RH_{SA}, Mixed air relative humidity RH_{MA}, Cooling coil outlet air relative humidity $RH_{A,out,CC}$, Post-heating coil outlet air relative humidity $RH_{A,out,PostHC}$ [47]	0 ÷ 100%	±3.00%
Outside air relative humidity RH_{OA} [48]	0 ÷ 100%	$\pm (2.3 + 0.008 \cdot RH_{OA})$%
Air relative humidity inside the integrated test room RH_{Room} [49]	0 ÷ 95%	±3.00%
Pre-heating coil heat carrier fluid volumetric flow rate $\dot{V}_{F,in,PreHC}$, Cooling coil heat carrier fluid volumetric flow rate $\dot{V}_{F,in,CC}$, Post-heating coil heat carrier fluid volumetric flow rate $\dot{V}_{F,in,PostHC}$ [51]	0.70 ÷ 2.34 m^3/h	±2.00% of reading
Percentage by volume of ethylene glycol in the heat carrier fluid entering the pre-heating coil $\%V_{Glycol,PreHC}$, Percentage by volume of ethylene glycol in the heat carrier fluid entering the cooling coil $\%V_{Glycol,CC}$, Percentage by volume of ethylene glycol in the heat carrier fluid entering the post-heating coil $\%V_{Glycol,PostHC}$ [51]	0 ÷ 100%	±5.00% of reading

2.2 Control logics of the AHU

The AHU is operated according to a specific control logic. Table 4 describes the conditions controlling the activation and deactivation of the main components of the AHU, whatever the period of the year is. Even if the AHU is equipped with the PreHC, this component has always been manually de-activated and not used during the experiments performed in this study.

Table 4. Conditions for activating/deactivating the main AHU components.

	ON	OFF
Humidifier (HUM)	$RH_{RA} \leq (RH_{SP,Room} - DB_{RH})$	$RH_{RA} \geq (RH_{SP,Room} + DB_{RH})$
Cooling coil (CC)	$T_{RA} \geq (T_{SP,Room} + DB_T)$ OR $RH_{RA} \geq (RH_{SP,Room} + DB_{RH})$	$T_{RA} \leq (T_{SP,Room} - DB_T)$ AND $RH_{RA} \leq (RH_{SP,Room} - DB_{RH})$
Post-heating coil (PostHC)	$T_{RA} \leq (T_{SP,Room} - DB_T)$	$T_{RA} \geq (T_{SP,Room} + DB_T)$
Heat Pump (HP)	$T_{HT} < (T_{HT,set\text{-}point} - 1\ °C)$	$T_{HT} \geq (T_{HT,set\text{-}point} + 1\ °C)$
Refrigerating System (RS)	$T_{CT} > (T_{CT,set\text{-}point} + 1\ °C)$	$T_{CT} \leq (T_{CT,set\text{-}point} - 1\ °C)$

At the beginning of the tests, the following parameters are manually set (and they could be eventually modified during the test) by the end-users: (i) the desired targets of both indoor air temperature ($T_{SP,Room}$) and relative humidity ($RH_{SP,Room}$) to be achieved inside the integrated test room; (ii) the deadbands DB_T and DB_{RH} of both $T_{SP,Room}$ and $RH_{SP,Room}$, respectively; (iii) the velocity (between 0% and 100%) of both the return air fan (OL_{RAF})

and the supply air fan (OL_{SAF}); (iv) the opening percentages (between 0% and 100%) of the return air damper (OP_{DRA}), the outside air damper (OP_{DOA}) and the exhaust air damper (OP_{DEA}); (v) the activation/deactivation of the static heat-recovery system damper by means of the opening percentage of the heat-recovery system damper (OP_{DHRS}).
Once the previous parameters are manually set by the end-users:

- the refrigeration machine operates to maintain a temperature T_{CT} equal to $T_{CT,set\text{-}point}$ (with a deadband of 1 °C) inside the 75-liter cold tank, while the heat pump is activated in order to achieve a temperature T_{HT} equal to $T_{HT,set\text{-}point}$ (with a deadband of 1 °C) inside the 75-liter hot tank;
- the desired return air temperature and relative humidity are kept at a chosen set-point (with defined deadbands) by regulating both the supply air temperature and the supply air relative humidity, while maintaining a constant air flow rate to the room;
- PID (proportional-integral-derivative) controllers automatically adjust (in the range 0÷100%) the opening percentages of the valves (OP_{V_PreHC}, OP_{V_PostHC}, OP_{V_CC} and OP_{V_HUM}) supplying the pre-heating coil, the post-heating coil, the cooling coil and the humidifier, respectively, with the aim of achieving the desired targets inside the test room;
- if the actual return air temperature T_{RA} is beyond the upper deadband UDB_T of the indoor air temperature setpoint $T_{SP,Room}$ ($UDB_T = T_{SP,Room} + DB_T$), the cooling coil valve PID loop is enabled and the cooling coil valve position is controlled in the range 0÷100% by the cooling coil valve controller PID output in order to achieve the lower deadband LDB_T ($LDB_T = T_{SP,Room} - DB_T$) of the indoor air temperature setpoint thanks to the reduction of supply air temperature; once this desired temperature level is reached, the post-heating coil is activated in order to increase the return air temperature up to the UDB_T by enhancing the supply air temperature; then, the cooling coil is activated again in order to reach the LDB_T and so forth; therefore, the HVAC system aims at maintaining the return air temperature between LDB_T and UDB_T, whatever the season is;
- when the actual return air temperature T_{RA} falls below the LDB_T, the cooling coil valve PID loop is disabled and the cooling coil valve is fully closed, except in the case when the indoor relative humidity has to be reduced;
- in the case of the actual return air temperature T_{RA} falls below the LDB_T, the heating coil valve PID loop is enabled and the heating coil valve position is regulated between 0 and 100% by the heating coil valve controller PID output in order to achieve a temperature level equal to the UDB_T by increasing the supply air temperature; once this desired temperature level is reached, the cooling coil is activated in order to reduce the return air temperature down to the LDB_T by lowering the supply air temperature; then, the heating coil is activated again in order to reach the UDB_T and so forth; therefore, the HVAC system aims at maintaining the return air temperature between LDB_T and UDB_T, whatever the season is;
- when the actual return air temperature T_{RA} is beyond the UDB_T, the heating coil valve PID loop is disabled and the heating coil valve is fully closed;
- in the case of the actual return air relative humidity RH_{RA} is beyond the upper deadband UDB_{RH} of the indoor air relative humidity setpoint $RH_{SP,Room}$ ($UDB_{RH} = RH_{SP,Room} + DB_{RH}$), the cooling coil valve PID loop is enabled and the cooling coil valve position is managed in the range 0÷100% by the cooling coil valve controller PID output in order to achieve the lower deadband LDB_{RH} of the indoor air relative humidity setpoint $RH_{SP,Room}$ ($LDB_{RH} = RH_{SP,Room} - DB_{RH}$); once this relative humidity is reached, the humidifier valve PID loop is enabled and the humidifier valve position is varied in the range 0÷100% by the humidifier valve controller PID in order to increase the return air relative humidity up to the UDB_{RH}; then, the cooling coil is activated again in order to reach the LDB_{RH} and so forth; therefore, the HVAC system aims at maintaining the return air relative humidity between LDB_{RH} and UDB_{RH}, whatever the season is;
- if the actual return air relative humidity RH_{RA} falls below the LDB_{RH}, the humidifier valve PID loop is enabled and the humidifier valve position is controlled between 0 and 100% by the humidifier valve controller PID output with the aim of achieving an indoor air relative humidity level equal to the UDB_{RH} while the cooling coil valve PID loop is disabled and the cooling coil valve is fully closed (except the case when indoor air temperature has to be reduced); once this relative humidity level is achieved, the cooling coil is activated in order to reduce the return air relative humidity down to the level LDB_{RH}; then, the humidifier is activated again in order to reach the indoor air relative humidity of UDB_{RH} and so forth; therefore, the HVAC system aims at keeping the return air relative humidity between LDB_{RH} and UDB_{RH}, whatever the season is.

However, alternatively the end-users are allowed to alter the components' operation/control logic based on specific research purposes by manually forcing (at the beginning or during the tests) the opening percentages of the valves in order to keep the desired user-defined positions. In addition, the end-users can manually vary the velocity of both supply and return air fans between 0% and 100%. Similarly, the parameters OP_{DRA}, OP_{DOA} and OP_{DEA} can be artificially forced in the range 0÷100%, where 100% means that the damper is fully open. The parameter OP_{DHRS} can be set to 100% (no heat recovery) or 0% (heat recovery takes place).

3. Experimental tests

Twenty-three fault free and faulty experiments have been carried out in order to investigate the behaviour of the AHU of the SENS i-Lab under Italian summer and winter. In particular, eleven tests (NS1, NS2, NS3, NS4, NS5, NS6, NW1, NW2, NW3, NW4 and NW5) have been performed under normal (N) operating conditions (i.e, without faults); in more detail, the tests (NS1, NS2, NS3, NS4, NS5 and NS6) have been performed during the summer 2021 (S), while the other tests (NW1, NW2, NW3, NW4 and NW5) have been carried out during the winter 2021/22 (W). The remaining twelve tests (FS1, FS2, FS3, FS4, FS5, FS6, FW1, FW2, FW3, FW4, FW5 and FW6) have been carried out during the summer 2021 (S) or the winter 2021/22 (W) while forcing the operation of specific AHU components/sensors (return air temperature sensor, return air relative humidity sensor, supply air fan, return air fan) in order to artificially simulate 6 specific typical faults. A single fault severity has been considered for each type of fault; in addition, faults have been investigated one by one and, therefore, no tests comprised multiple faults occurring simultaneously.

Table 5 describes the operating conditions of the fault free tests, while Table 6 details the operating conditions of the faulty tests (where the cells corresponding to the faulty component have been highlighted by a yellow shade). In particular, Tables 5 and 6 indicate for each test the values of $T_{SP,Room}$, $RH_{SP,Room}$, DB_T, DB_{RH}, OL_{SAF}, OL_{RAF}, OP_{V_PostHC}, OP_{V_CC}, OP_{V_HUM}, OP_{DRA}, OP_{DHRS}, OP_{DOA}, OP_{DEA} as well as the date associated to the fault free tests and faulty tests, respectively. All tests have been started at 9:00 a.m. and ended at 6:00 p.m., without activating the pre-heating coil. Both fault free and faulty experiments have been performed without internal gains/loads (i.e., lighting systems switched off and no one inside the test room). A value of about 6% has been measured as percentage by volume of ethylene glycol in the heat carrier fluid entering the pre-heating/cooling/post-heating coil during the tests.

Table 5. Operating conditions of the fault free tests.

	NS1	**NS2**	**NS3**	**NS4**	**NS5**	**NS6**	**NW1**	**NW2**	**NW3**	**NW4**	**NW5**
$T_{SP,Room}$ (°C)	26						20				
$RH_{SP,Room}$ (%)	50										
DB_T (°C)	1										
DB_{RH} (%)	5										
OL_{SAF} (%)	50										
OL_{RAF} (%)	50										
OP_{V_PostHC} (%)	0 ÷ 100										
OP_{V_CC} (%)	0 ÷ 100										
OP_{V_HUM} (%)	0 ÷ 100										
OP_{DRA} (%)	100										
OP_{DHRS} (%)	100										
OP_{DOA} (%)	20										
OP_{DEA} (%)	20										
Date (dd/mm/yy)	14/07/21	06/08/21	23/07/21	27/07/21	31/08/21	09/09/21	14/01/22	22/12/21	17/02/22	30/12/21	15/12/21

Table 6. Operating conditions of the faulty tests.

	FS1	FW1	FS2	FW2	FS3	FW3	FS4	FW4	FS5	FW5	FS6	FW6
$T_{SP,Room}$ (°C)	26	20	26	20	26	20	26	20	26	20	26	20
$RH_{SP,Room}$ (%)	50											
DB_T (°C)	1											
DB_{RH} (%)	5											
Offset of T_{RA} sensor (°C)	+3	+3	–3	–3	0	0	0	0	0	0	0	0
Offset of RH_{RA} sensor (%)	0	0	0		+15	+15	–15	–15	0		0	
OL_{SAF} (%)	50	50	50	50	50	50	50	50	50	50	0	0
OL_{RAF} (%)	50	50	50	50	50	50	50	50	0	0	50	50
OP_{V_PostHC} (%)	0 ÷ 100											
OP_{V_CC} (%)	0 ÷ 100											
OP_{V_HUM} (%)	0 ÷ 100											
OP_{DRA} (%)	100											
OP_{DHRS} (%)	100											
OP_{DOA} (%)	20											
OP_{DEA} (%)	20											
Date (dd/mm/yy)	05/08/21	02/02/22	02/08/21	21/12/21	22/07/21	16/02/22	26/07/21	29/12/21	07/09/21	20/12/21	08/09/21	17/12/21

With reference to the fault free tests, the target of the return air temperature has been set at 26 °C during the summer and 20 °C during the winter (with a deadband of 1 °C), while the target associated to the return air relative humidity is 50% during both seasons (with a deadband of 5%). In addition, during the normal experiments, the values of OL_{SAF}, OL_{RAF}, OP_{DRA}, OP_{DHRS}, OP_{DOA} and OP_{DEA} have been set equal to 50%, 50%, 100%, 100%, 20% and 20%, respectively, according to the guidelines indicated by the designer of the HVAC system. Finally, a healthy operation of all valves has been allowed with values of OP_{V_PostHC}, OP_{V_CC}, OP_{V_PretHC} and OP_{V_HUM} in the range 0 ÷ 100%.

The values of $T_{SP,Room}$, $RH_{SP,Room}$, DB_T, DB_{RH}, OP_{DRA}, OP_{DHRS}, OP_{DOA} and OP_{DEA} during the faulty tests have been maintained equal to the values set during the fault free tests. Six faults have been artificially introduced at the beginning of the faulty tests and continuously maintained during their entire durations (from 9:00 am up to 6:00 pm) with no interruptions during the experiments. In greater detail:

- the fault 1, corresponding to the case of a positive offset equal to +3.0 °C purposely added on the return air temperature sensor, has been implemented during the faulty tests FS1 and FW1;
- the fault 2, corresponding to the case of a negative offset equal to –3.0 °C artificially subtracted from the values measured by return air temperature sensor, has been implemented during the faulty tests FS2 and FW2;
- the fault 3, corresponding to the case of a positive offset of the return air relative humidity sensor kept equal to +15 %, has been artificially implemented during the faulty tests FS3 and FW3;
- the fault 4, corresponding to the case of a negative offset of the return air relative humidity sensor kept constant and equal to –15% has been artificially implemented during the faulty tests FS4 and FW4;
- the fault 5, corresponding to a complete failure of the return air fan (instead of a nominal velocity of 50%), has been artificially implemented during the faulty tests FS5 and FW5;
- the fault 6, corresponding to a complete failure of the supply air fan (instead of a nominal velocity of 50%), has been artificially implemented during the faulty tests FS6 and FW6.

The sensors' offsets (faults 1, 2, 3 and 4) have been artificially implemented by increasing or decreasing the sensors' output; in other words, the AHU controller receives an increased or decreased return air temperature or relative humidity with respect to the real/actual values and regulates the AHU operation based on faulty sensors' readings. The faults 5 and 6 have been artificially introduced by forcing at 0% the associated command signal trying to regulate the speed of the return air fan and supply air fan, respectively.
All the parameters indicated in Table 3 have been measured every second during all normal and faulty tests.
During the experiments, the outside air temperature ranged from a minimum of 21.5 °C up to a maximum of 41.9 °C during the summer and from a minimum of 6.2 °C up to a maximum of 24.4 °C during the winter; the outside air relative humidity varied in the range 18.9%÷71.4% during the summer and in the range 21.6%÷90.6% during the winter.

4. Comparison of boundary conditions during fault free and faulty tests

The tests under normal conditions (NS1-NS6 and NW1-NW5) have been assumed as baselines to be compared with the faulty tests (FS1-FS6 and FW1-FW6) in order to discover and highlight the impact of the investigated faults. In particular, all the normal and faulty tests have been started at 9 a.m. by maintaining the same initial return air temperature $T_{RA,initial}$ (about 28 °C for summer tests and 18 °C for winter tests) and initial return air relative humidity $RH_{RA,initial}$ (about 60% for both summer and winter tests). The comparability of the healthy experiments with the corresponding faulty ones has been verified by contrasting the boundary conditions occurring during the tests in terms of outside air temperature T_{OA} and outside air relative humidity RH_{OA} by means of the following metrics:

$$\varepsilon_i = EXP_{OA,Baseline,i} - EXP_{OA,Faulty,i} \quad (1)$$

$$\overline{\varepsilon} = \sum_{i=1}^{N} \frac{\varepsilon_i}{N} \quad (2)$$

$$\left|\overline{\varepsilon}\right| = \sum_{i=1}^{N} \frac{\left|\varepsilon_i\right|}{N} \quad (3)$$

$$RMSD = \sqrt{\sum_{i=1}^{N} \frac{\left(\varepsilon_i - \overline{\varepsilon}\right)^2}{N}} \quad (4)$$

where $\overline{\varepsilon}$ is the average difference, $\left|\overline{\varepsilon}\right|$ is the average absolute difference, RMSD is the root mean square difference, N is the number of experimental data points of each single test, $EXP_{OA,Baseline,i}$ and $EXP_{OA,Faulty,i}$ are, respectively, the experimental values of T_{OA} and RH_{OA} at time step i under healthy and faulty conditions. Table 7 summarizes the values of $\overline{\varepsilon}$, $\left|\overline{\varepsilon}\right|$ and RMSD as result of the comparisons of the most similar fault free and faulty experiments among the above-mentioned tests in terms of T_{OA} and RH_{OA}. In Table 7 the worst values of $\overline{\varepsilon}$, $\left|\overline{\varepsilon}\right|$ and RMSD are highlighted by red font, while the best values (i.e., closest to 0) of $\overline{\varepsilon}$, $\left|\overline{\varepsilon}\right|$ and RMSD are denoted by green font.

Table 7. Comparison of healthy and faulty tests in terms of outside air temperature T_{OA} and outside air relative humidity RH_{OA}.

Fault free against faulty tests	T_{OA} (°C)			RH_{OA} (%)		
	$\bar{\varepsilon}$	$\lvert\bar{\varepsilon}\rvert$	RMSD	$\bar{\varepsilon}$	$\lvert\bar{\varepsilon}\rvert$	RMSD
Normal test NS1 vs. faulty test FS1	0.0	0.7	0.9	–4.8	5.0	3.7
Normal test NS2 vs. faulty test FS2	–0.4	0.8	0.9	3.4	3.9	3.1
Normal test NS3 vs. faulty test FS3	–0.1	0.8	0.9	1.5	4.5	4.7
Normal test NS4 vs. faulty test FS4	0.1	0.7	0.9	–1.2	3.7	4.3
Normal test NS5 vs. faulty test FS5	–0.6	0.7	0.9	4.2	4.8	3.8
Normal test NS6 vs. faulty test FS6	–0.6	0.9	0.9	1.6	2.4	2.5
Normal test NW1 vs. faulty test FW1	–1.1	1.4	1.5	7.1	8.0	9.3
Normal test NW2 vs. faulty test FW2	0.6	1.0	0.9	–2.0	3.6	3.9
Normal test NW3 vs. faulty test FW3	0.3	1.2	1.4	–2.5	3.4	3.5
Normal test NW4 vs. faulty test FW4	–0.2	0.8	1.0	–8.7	8.7	4.0
Normal test NW5 vs. faulty test FW5	0.8	1.3	1.3	–3.6	4.6	4.7
Normal test NW5 vs. faulty test FW6	–0.6	1.0	1.3	–0.8	4.0	4.9

Table 7 highlights how the values of $\bar{\varepsilon}$, $\lvert\bar{\varepsilon}\rvert$ and RMSD are, respectively, at most –1.1 °C, 1.4 °C, 1.5 °C for T_{OA} and –8.7%, 8.7%, 9.3% for RH_{OA}. The results reported in this table indicate that the values of $\lvert\bar{\varepsilon}\rvert$ are always not larger than 1.5 °C with respect to T_{OA} and not larger than 10.0% with respect to RH_{OA}; therefore, according to approach suggested in [20], the boundary conditions of the contrasted fault free and faulty tests can be considered as very similar; as a consequence, comparing the above-mentioned healthy and faulty experiments (NS1 vs. FS1, NS2 vs. FS2, NS3 vs. FS3, NS4 vs. FS4, NS5 vs. FS5, NS6 vs. FS6, NW1 vs. FW1, NW2 vs. FS2, NW3 vs. FW3, NW4 vs. FW4, NW5 vs. FW5, NW5 vs. FW6) is possible for assessing the impact of each investigated fault on the AHU behaviour/performance. In the Appendix A the normal tests and the corresponding faulty tests are compared in terms of temporal trends of outside air temperature/relative humidity as well as initial return air conditions.

5. Faults' symptoms: results and discussion

In this section, the healthy tests and the corresponding faulty tests are compared to highlight the impact of each investigated fault on the AHU behaviour/performance. The comparison is performed from different points of view. In particular, the subsection 5.1 reports the effects of the selected faults on indoor thermal/hygrometric comfort, while the subsection 5.2 focuses on the experimental patterns of AHU key operating parameters and symptom occurrence probability.

5.1 Effects of faults on thermal and hygrometric comfort

Table 8 compares the thermal/hygrometric comfort time (i.e., the percentage of time with values of indoor air temperature/relative humidity within the given deadbands over the entire test duration) of the experimental tests without faults as well as the corresponding faulty ones. In addition, Table 8 shows the parameters $\lvert\bar{\varepsilon}_{T,D}\rvert$ and $\lvert\bar{\varepsilon}_{RH,D}\rvert$ calculated according to the experimental data by means of the following formulas:

$$\lvert\bar{\varepsilon}_{T,D}\rvert = \sum_{i=1}^{N} \lvert\Delta T_{out,DBT}\rvert / N_{out,DBT} \quad (5)$$

$$\lvert\bar{\varepsilon}_{RH,D}\rvert = \sum_{i=1}^{N} \lvert\Delta RH_{out,DBRH}\rvert / N_{out,DBRH} \quad (6)$$

where: $\Delta T_{out,DBT}$ represents the difference between the actual return air temperature T_{RA} and the upper deadband UDB_T calculated only in the cases where T_{RA} is larger than UDB_T, or the difference between the lower deadband LDB_T and the actual return air temperature T_{RA} evaluated only when T_{RA} is lower than LDB_T; $\Delta RH_{out,DBRH}$ represents the difference between the actual return air relative humidity RH_{RA} and the upper deadband UDB_{RH} calculated only in the cases where RH_{RA} is larger than UDB_{RH}, or the difference between the lower deadband LDB_{RH} and the actual return air relative humidity RH_{RA} evaluated only when RH_{RA} is

lower LDB_{RH}; $N_{out,DBT}$ and $N_{out,DBRH}$ are the number of experimental data points with T_{RA} and RH_{RA} out of the corresponding deadbands, respectively. The parameters $\left|\overline{\varepsilon}_{T,D}\right|$ and $\left|\overline{\varepsilon}_{RH,D}\right|$ allow to characterize the relevance of thermal/hygrometric discomfort (the greater the values of $\left|\overline{\varepsilon}_{T,D}\right|$ and $\left|\overline{\varepsilon}_{RH,D}\right|$, the greater the relevance of thermal and hygrometric discomfort, respectively). In Table 8 the worst results are highlighted by red font, while the best data are denoted by green font.

Table 8. Thermal-hygrometric comfort time with and without faults.

ID test	Thermal comfort time (%)	$\left\|\overline{\varepsilon}_{T,D}\right\|$ (°C)	Hygrometric comfort time (%)	$\left\|\overline{\varepsilon}_{RH,D}\right\|$ (%)
Faulty test FS1	2.45	1.87	59.38	6.40
Normal test NS1	68.79	0.30	83.59	7.41
Faulty test FW1	0.00	1.64	95.75	4.71
Normal test NW1	78.22	0.53	92.46	4.65
Faulty test FS2	0.00	2.14	75.44	5.82
Normal test NS2	74.81	0.30	91.83	5.99
Faulty test FW2	8.22	1.95	86.80	5.20
Normal test NW2	75.17	0.18	95.35	5.48
Faulty test FS3	76.03	0.13	25.38	6.20
Normal test NS3	71.59	0.36	92.17	5.79
Faulty test FW3	76.38	0.26	93.30	7.14
Normal test NW3	76.34	0.26	95.32	5.50
Faulty test FS4	88.09	0.36	0.65	15.85
Normal test NS4	76.00	0.37	89.92	6.52
Faulty test FW4	71.99	0.46	0.00	12.69
Normal test NW4	78.03	0.19	90.87	5.42
Faulty test FS5	70.47	0.29	86.04	7.36
Normal test NS5	69.40	0.32	86.21	7.08
Faulty test FW5	76.33	0.28	89.56	6.54
Normal test NW5	75.78	0.17	96.84	5.23
Faulty test FS6	58.67	0.23	31.29	5.23
Normal test NS6	77.32	0.16	93.31	7.84
Faulty test FW6	74.79	0.15	98.13	5.20
Normal test NW5	75.78	0.17	96.84	5.23

It should be highlighted that the thermal/hygrometric comfort time associated to the normal tests is lower than 100% because of the facts that: (a) the initial values of the return air temperature and the return air relative humidity are far from the given target values (and, therefore, a relevant time is required to achieve the desired targets from the beginning of the tests); (b) during the start-up phases the AHU operates under transient conditions trying to approach the steady-state performance.
Figure 4 reports the difference between faulty and normal tests in terms of both thermal comfort time ($\%DCT_T$) and hygrometric comfort time ($\%DCT_{RH}$):

$$\%DCT_T = TCT_{Faulty,T} - TCT_{Baseline,T} \quad (7)$$

$$\%DCT_{RH} = HCT_{Faulty,RH} - HCT_{Baseline,RH} \quad (8)$$

where $TCT_{Faulty,T}$ and $TCT_{Baseline,T}$ are, respectively, the thermal comfort time during faulty and corresponding normal tests, while $HCT_{Faulty,RH}$ and $HCT_{Baseline,RH}$ correspond to the hygrometric comfort time during faulty and corresponding normal tests, respectively. A negative value of $\%DCT_T$ or $\%DCT_{RH}$ means that the thermal or the hygrometric comfort time associated with the faulty test is lower than the corresponding normal test.

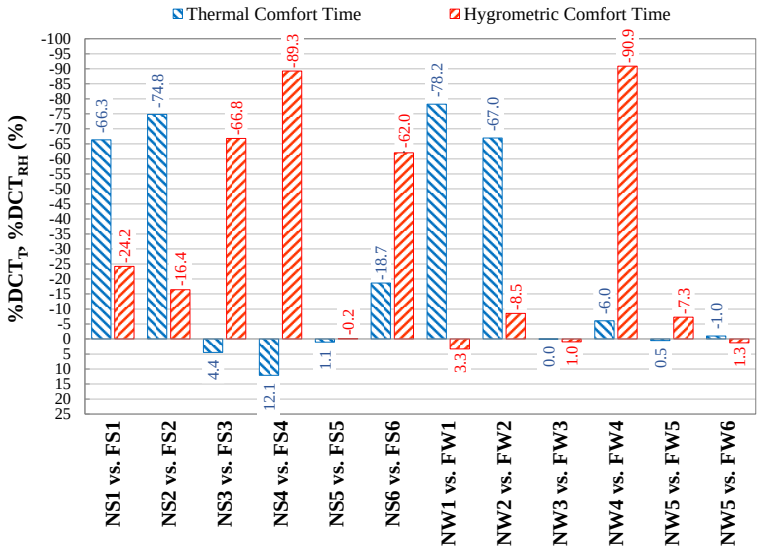

Figure 4. Difference between faulty tests and baselines in terms of thermal and hygrometric comfort time.

In comparison to the normal tests, Table 8 and Figure 4 highlight that:

- the occurrence of the fault 1 (i.e., positive offset equal to +3.0 °C of the return air temperature sensor) strongly reduces thermal comfort time (–66.3% during summer and –78.2% during winter) due to the wrong measurement of the actual return air temperature (measured value greater than the real one); a significant reduction of hygrometric comfort time is observed only during summer (–24.2%), while during winter there is a negligible variation of hygrometric comfort time (+3.3%). The fault 1 also implies a relevant intensity of thermal discomfort considering that $\left|\overline{\varepsilon}_{T,D}\right|$ is equal to 1.87 °C during summer and 1.64 °C during winter;
- during both summer and winter, the fault 2 (i.e., negative offset of the return air temperature sensor equal to –3.0 °C) significantly reduces thermal comfort time (–74.8% and –67.0%, respectively), together with a not negligible variation of hygrometric comfort time (–16.4% and –8.5%, respectively); these results are related to the fact that the actual return air temperature is not correctly measured (measured value lower than the real one); the significance of thermal discomfort is important also in the case of the fault 2 (taking into account that $\left|\overline{\varepsilon}_{T,D}\right|$ = 2.14 °C during summer and $\left|\overline{\varepsilon}_{T,D}\right|$ = 1.95 °C during winter);
- during summer, the occurrence of the fault 3 (i.e., the positive offset of the return air relative humidity sensor equal to +15%) does not imply a relevant difference in terms of thermal comfort time (+4.4%), while it strongly reduces (–66.8%) hygrometric comfort time (due to the fact that real return air relative humidity is greater than the measured one); during winter, the fault 3 is characterized by a negligible variation in terms of both thermal comfort time (0.0%) and hygrometric comfort time (+1.0%); this fault also implies a not insignificant intensity of hygrometric discomfort considering that $\left|\overline{\varepsilon}_{RH,D}\right|$ is equal to 6.20% during summer and equal to 7.14% during winter;
- the fault 4 (i.e., negative offset of the return air relative humidity sensor equal to –15%) causes a strong reduction of hygrometric comfort time (–89.3% and –90.9% during summer and winter, respectively) for the reason that the measured return air relative humidity value is lower than the real one. The occurrence of the fault 4 is also characterized by a substantial importance of hygrometric discomfort according to the values of $\left|\overline{\varepsilon}_{RH,D}\right|$ equal to 15.85% and 12.69% during summer and winter, respectively;
- negligible effects on both thermal comfort time (+1.1% and +0.5% during winter) and hygrometric comfort time (–0.2% during summer and –7.3% during winter) are associated with the fault 5 (i.e., complete failure of the return air fan) as a consequence of the fact that the AHU is still able to guarantee the desired indoor air temperature and relative humidity (thanks to the operation of the supply air fan);
- the occurrence of the fault 6 (i.e., complete failure of the supply air fan) during summer highlights a lower thermal comfort time (–18.7%), together with a really relevant reduction of hygrometric comfort time (–62.0%), due to the fact that the air supply is compromised; during winter, the fault 6 highlights a negligible variation of both thermal comfort time (–1.0%) and hygrometric comfort time (+1.3%).

5.2 Effects of faults on the patterns of key operating parameters

The assessment of faults' effects on AHU key operating parameters is of paramount importance in order to (i) assess the gaps between AHU faulty operation and design expectations, (ii) identify the most impacted operational parameters and (iii) select the threshold tolerance values required by data-driven rule-based AFDD methods. The differences between the values measured during the fault free tests and the values measured during the corresponding faulty experiments of AHU key operating parameters (T_{RA}, T_{MA}, $T_{A,out,CC}$, $T_{A,out,PostHC}$, T_{SA}, RH_{RA}, RH_{MA}, $RH_{A,out,CC}$, $RH_{A,out,PostHC}$, RH_{SA}, $T_{F,out,CC}$, $T_{F,in,CC}$, $T_{F,out,PostHC}$, $T_{F,in,PostHC}$, $\dot{V}_{F,in,CC}$ and $\dot{V}_{F,in,PostHC}$) are compared in Figures B.1, B.2 and B.3 of the Appendix B. According to [22,52], the above-mentioned key variables considered in this experimental study are easily available in practical AHUs and reflect measurements that are typically logged in building control systems that AFDD tools generally have access to. In this section, the comparison between the normal and the corresponding faulty tests is performed by contrasting the arithmetic mean μ as well as the standard deviation σ of the above-mentioned parameters calculated as follows:

$$\mu = \sum_{i=1}^{N} \frac{d_i}{N} \tag{9}$$

$$\sigma = \sqrt{\sum_{i=1}^{N} \frac{(d_i - \mu)^2}{N}} \tag{10}$$

where N is the number of experimental points of a single test and d_i is the experimental value at time step i of the test.

The approach of this study is fully consistent with that one adopted in several scientific papers [20,32] to assess symptom patterns according to various faults and boundary conditions. In particular, Wen and Li [20] performed a fault impact analysis by comparing the fault free and faulty operation of a VAV AHU during winter, spring and summer in Iowa (U.S.A.) in terms of arithmetic mean and standard deviation of the most important key operating parameters. According to [32], the symptom associated to a fault can be detected by comparing faulty and fault free tests performed under the same boundary conditions in the case of the absolute difference between each observation during faulty condition $y_{i,Faulty}$ and the arithmetic mean of measurements under normal operation $\mu_{Baseline}$ is higher than the standard deviation under fault free scenarios $\sigma_{Baseline}$ according to the following equation:

$$\left| y_{i,Faulty} - \mu_{Baseline} \right| > t \cdot \sigma_{Baseline} \tag{11}$$

where t is the threshold value that can be set equal to one (with a 68% confidence level); a lower threshold implies that a smaller deviation of faulty observations from normal conditions can be captured and classified as symptom event. However, it should be underlined that fault symptom magnitude could also be affected by several factors, such as climatic conditions, thermal/cooling loads as well as system control logic; that's the reason why in this work the selected faults have been investigated during both winter and summer.

The values of μ and σ calculated in this study based on the experimental data gathered during fault free and faulty tests are reported in Tables 9, 10 and 11. In particular, Table 9 refers to the parameters T_{RA}, T_{MA}, $T_{A,out,CC}$, $T_{A,out,PostHC}$ and T_{SA}; Table 10 corresponds to the parameters RH_{RA}, RH_{MA}, $RH_{A,out,CC}$, $RH_{A,out,PostHC}$ and RH_{SA}; finally, Table 11 focuses on the parameters $T_{F,out,CC}$, $T_{F,in,CC}$, $T_{F,out,PostHC}$, $T_{F,in,PostHC}$, $\dot{V}_{F,in,CC}$ and $\dot{V}_{F,in,PostHC}$. These tables also show the difference Δ between the values of the arithmetic mean and the standard deviation associated to the above-mentioned 16 key operating parameters calculated during the faulty tests with respect to those obtained during the corresponding fault free experiments. This difference has been calculated by means of the following formula:

$$\Delta = X_{Faulty} - X_{Baseline} \tag{12}$$

where X_{Faulty} and $X_{Baseline}$ represent the arithmetic mean or the standard deviation of the 16 above-mentioned parameters under faulty and healthy conditions, respectively. A value of Δ equal to 0 means that there is no difference between the corresponding faulty and fault free tests in terms of arithmetic mean and standard

deviation. For each row corresponding to the values of the parameter Δ (Eq. 12) in Tables 9-11, the largest/worst absolute values of μ and σ are highlighted by red font, while the values of μ and σ closest to 0 are denoted by green font.

Table 9. Differences between faulty and normal tests in terms of T_{RA}, T_{MA}, $T_{A,out,CC}$, $T_{A,out,PostHC}$ and T_{SA}.

ID Test	T_{RA}		T_{MA}		$T_{A,out,CC}$		$T_{A,out,PostHC}$		T_{SA}	
	μ (°C)	σ (°C)	μ (°C)	σ (°C)	μ (°C)	σ (°C)	μ (°C)	σ (°C)	μ (°C)	σ (°C)
NS1	26.19	0.85	28.24	1.13	12.74	3.15	23.74	8.16	26.12	6.10
FS1	23.30	1.14	26.64	0.48	10.70	1.00	16.89	7.50	19.68	6.13
$\Delta_{FS1\ vs.\ NS1}$	-2.89	0.29	-1.60	-0.65	-2.05	-2.15	-6.85	-0.67	-6.45	0.03
NS2	26.34	0.81	28.72	1.29	11.72	2.31	24.09	8.06	26.66	6.27
FS2	29.14	0.71	30.09	1.29	14.16	3.87	29.56	5.91	31.70	4.52
$\Delta_{FS2\ vs.\ NS2}$	2.80	-0.10	1.36	0.00	2.44	1.57	5.47	-2.15	5.04	-1.76
NS3	26.36	0.85	29.60	1.44	12.09	2.67	23.44	8.08	26.22	6.23
FS3	26.23	0.76	29.55	1.31	10.81	0.71	23.83	7.59	26.47	5.72
$\Delta_{FS3\ vs.\ NS3}$	-0.13	-0.08	-0.05	-0.12	-1.29	-1.96	0.39	-0.50	0.25	-0.50
NS4	26.36	0.78	30.66	1.55	12.01	3.05	25.20	7.92	27.92	6.16
FS4	25.80	0.78	30.05	1.53	12.30	3.45	20.77	6.13	24.27	4.85
$\Delta_{FS4\ vs.\ NS4}$	-0.56	0.00	-0.61	-0.02	0.29	0.41	-4.43	-1.79	-3.66	-1.31
NS5	26.24	0.85	29.03	1.38	12.45	3.10	22.78	8.22	25.42	6.23
FS5	26.23	0.84	31.00	2.79	11.93	2.89	23.91	8.47	26.63	6.56
$\Delta_{FS5\ vs.\ NS5}$	-0.02	-0.01	1.97	1.41	-0.51	-0.20	1.13	0.25	1.21	0.33
NS6	26.23	0.78	28.68	1.56	10.66	0.81	23.55	7.68	26.16	5.81
FS6	27.06	0.22	28.21	1.25	10.13	0.89	15.58	2.31	21.34	2.05
$\Delta_{FS6\ vs.\ NS6}$	0.83	-0.55	-0.48	-0.31	-0.52	0.08	-7.97	-5.37	-4.82	-3.76
NW1	20.02	0.94	19.06	1.85	9.66	1.67	14.52	8.04	16.43	6.45
FW1	17.36	0.22	18.09	2.01	8.93	0.57	9.34	0.55	11.53	0.89
$\Delta_{FW1\ vs.\ NW1}$	-2.66	-0.72	-0.96	0.16	-0.72	-1.10	-5.18	-7.49	-4.90	-5.56
NW2	20.17	0.78	17.96	0.91	9.28	0.46	19.64	8.45	21.03	6.78
FW2	22.67	1.22	18.95	0.88	10.39	1.62	25.27	7.39	26.25	5.89
$\Delta_{FW2\ vs.\ NW2}$	2.50	0.44	0.99	-0.03	1.10	1.16	5.64	-1.06	5.21	-0.89
NW3	20.11	0.82	20.16	1.86	9.53	0.85	19.49	9.94	21.27	8.13
FW3	20.14	0.81	20.23	1.46	9.39	0.45	19.93	9.95	21.69	8.16
$\Delta_{FW3\ vs.\ NW3}$	0.03	-0.01	0.07	-0.40	-0.14	-0.40	0.44	0.01	0.42	0.04
NW4	20.10	0.78	20.41	1.57	9.65	0.42	20.00	8.73	21.70	7.10
FW4	20.24	0.91	20.60	1.46	11.04	2.10	18.04	8.37	20.17	6.59
$\Delta_{FW4\ vs.\ NW4}$	0.14	0.13	0.19	-0.12	1.39	1.68	-1.96	-0.35	-1.53	-0.51
NW5	20.14	0.79	19.72	1.54	9.31	0.46	18.30	8.37	20.05	6.63
FW5	20.15	0.80	16.30	2.53	9.50	1.68	20.57	9.16	22.11	7.61
$\Delta_{FW5\ vs.\ NW5}$	0.02	0.02	-3.43	0.99	0.19	1.22	2.27	0.79	2.06	0.98
NW5	20.14	0.79	19.72	1.54	9.31	0.46	18.30	8.37	20.05	6.63
FW6	20.28	0.75	20.43	1.63	9.97	0.92	29.99	12.85	28.46	10.13
$\Delta_{FW6\ vs.\ NW5}$	0.14	-0.04	0.71	0.09	0.65	0.46	11.69	4.49	8.42	3.50

Table 10. Differences between faulty and normal tests in terms of RH_{RA}, RH_{MA}, $RH_{A,out,CC}$, $RH_{A,out,PostHC}$ and RH_{SA}.

ID Test	RH_{RA}		RH_{MA}		$RH_{A,out,CC}$		$RH_{A,out,PostHC}$		RH_{SA}	
	μ (%)	σ (%)	μ (%)	σ (%)	μ (%)	σ (%)	μ (%)	σ (%)	μ (%)	σ (%)
NS1	50.30	4.27	48.77	5.04	99.46	1.35	58.53	21.79	54.62	16.17
FS1	54.64	2.88	52.78	3.80	95.49	3.04	75.30	25.85	63.42	17.87
$\Delta_{FS1\ vs.\ NS1}$	4.34	-1.39	4.01	-1.24	-3.97	1.70	16.77	4.06	8.80	1.70
NS2	49.43	3.45	49.39	4.08	94.18	3.11	54.52	23.95	49.21	16.11
FS2	49.99	4.29	49.39	4.96	95.45	3.75	46.31	17.72	47.96	19.19
$\Delta_{FS2\ vs.\ NS2}$	0.56	0.85	0.00	0.88	1.27	0.64	-8.21	-6.23	-1.25	3.08
NS3	49.69	3.30	49.33	4.85	99.00	1.99	57.09	23.58	51.24	15.69
FS3	43.90	2.39	44.94	3.38	99.38	1.15	50.66	23.32	43.61	13.60
$\Delta_{FS3\ vs.\ NS3}$	-5.79	-0.91	-4.39	-1.47	0.38	-0.84	-6.43	-0.26	-7.63	-2.09
NS4	49.47	3.60	42.09	4.37	99.19	1.51	51.58	22.43	46.33	15.51
FS4	66.77	3.58	51.65	5.72	99.71	1.78	85.18	21.43	82.70	20.75
$\Delta_{FS4\ vs.\ NS4}$	17.30	-0.02	9.56	1.35	0.52	0.26	33.60	-1.01	36.36	5.24
NS5	49.82	3.86	46.64	5.33	93.05	3.56	60.25	22.28	54.52	15.25
FS5	49.67	4.18	33.03	6.93	90.20	5.12	54.57	23.00	49.50	16.23
$\Delta_{FS5\ vs.\ NS5}$	-0.15	0.32	-13.60	1.60	-2.84	1.56	-5.69	0.72	-5.02	0.98
NS6	49.87	3.13	41.41	5.96	91.03	2.54	51.35	23.29	44.06	13.76
FS6	55.56	1.36	47.49	5.18	86.19	3.15	66.66	6.31	50.32	4.43
$\Delta_{FS6\ vs.\ NS6}$	5.69	-1.77	6.08	-0.79	-4.84	0.62	15.31	-16.98	6.27	-9.33
NW1	48.59	2.55	52.27	7.36	88.06	6.55	75.55	22.44	67.04	13.97
FW1	48.26	2.93	48.10	7.84	81.61	6.22	83.64	5.09	73.14	7.72
$\Delta_{FW1\ vs.\ NW1}$	-0.33	0.37	-4.17	0.48	-6.45	-0.33	8.08	-17.35	6.10	-6.25
NW2	48.63	2.80	58.31	3.67	92.41	2.16	60.91	27.46	55.36	20.18
FW2	49.11	3.35	60.64	3.66	92.66	2.95	48.07	21.61	47.13	15.61
$\Delta_{FW2\ vs.\ NW2}$	0.47	0.56	2.34	-0.01	0.24	0.79	-12.84	-5.85	-8.22	-4.57
NW3	49.49	2.59	54.31	7.51	94.09	1.92	64.08	29.31	55.73	20.52
FW3	49.55	2.50	54.80	6.26	94.85	1.15	63.07	29.91	54.96	21.02
$\Delta_{FW3\ vs.\ NW3}$	0.06	-0.09	0.49	-1.25	0.76	-0.76	-1.01	0.60	-0.77	0.51
NW4	52.24	2.09	58.60	6.15	94.02	1.64	62.40	28.19	54.88	19.33
FW4	63.69	3.50	68.51	6.03	94.13	2.18	76.83	23.71	71.99	17.06
$\Delta_{FW4\ vs.\ NW4}$	11.45	1.42	9.91	-0.12	0.11	0.54	14.43	-4.48	17.11	-2.27
NW5	49.64	2.41	54.47	5.50	92.66	1.70	66.08	27.23	58.13	18.96
FW5	49.30	3.58	60.90	8.74	86.36	7.14	56.47	27.58	52.63	20.95
$\Delta_{FW5\ vs.\ NW5}$	-0.34	1.16	6.43	3.25	-6.30	5.44	-9.61	0.35	-5.50	1.99
NW5	49.64	2.41	54.47	5.50	92.66	1.70	66.08	27.23	58.13	18.96
FW6	49.79	2.02	54.66	5.14	86.64	3.91	39.77	30.62	39.70	23.17
$\Delta_{FW6\ vs.\ NW5}$	0.15	-0.39	0.19	-0.36	-6.02	2.21	-26.32	3.40	-18.43	4.21

Table 11. Differences between faulty and normal tests in terms of $T_{F,out,CC}$, $T_{F,in,CC}$, $T_{F,out,PostHC}$, $T_{F,in,PostHC}$, $\dot{V}_{F,in,CC}$ and $\dot{V}_{F,in,PostHC}$.

ID Test	$T_{F,out,CC}$		$T_{F,in,CC}$		$T_{F,out,PostHC}$		$T_{F,in,PostHC}$		$\dot{V}_{F,in,CC}$		$\dot{V}_{F,in,PostHC}$	
	μ (°C)	σ (°C)	μ (°C)	σ (°C)	μ (°C)	σ (°C)	μ (°C)	σ (°C)	μ (m³/h)	σ (m³/h)	μ (m³/h)	σ (m³/h)
NS1	11.25	1.29	8.95	0.94	40.62	2.21	43.25	1.42	1.46	0.76	0.98	0.84
FS1	10.62	0.86	8.67	0.87	37.50	3.04	40.80	2.89	1.87	0.11	0.40	0.67
$\Delta_{FS1\ vs.\ NS1}$	-0.63	-0.44	-0.29	-0.07	-3.11	0.83	-2.45	1.46	0.40	-0.65	-0.58	-0.17
NS2	10.98	1.10	8.65	0.83	41.22	1.73	43.54	1.19	1.68	0.55	1.04	0.83
FS2	11.66	1.50	8.80	0.98	41.64	1.69	43.60	1.13	1.28	0.85	1.46	0.61
$\Delta_{FS2\ vs.\ NS2}$	0.68	0.40	0.15	0.16	0.42	-0.05	0.06	-0.05	-0.40	0.30	0.42	-0.22
NS3	11.10	1.30	8.57	1.04	40.74	2.30	43.20	1.38	1.64	0.60	0.98	0.85
FS3	10.60	0.72	8.40	0.74	40.85	1.92	43.39	1.28	1.87	0.09	1.05	0.83
$\Delta_{FS3\ vs.\ NS3}$	-0.51	-0.59	-0.17	-0.30	0.12	-0.38	0.19	-0.10	0.22	-0.51	0.07	-0.01
NS4	10.99	1.30	8.55	0.97	41.67	1.37	43.82	1.11	1.60	0.65	1.14	0.81
FS4	11.06	1.28	8.44	0.99	39.27	2.70	42.76	2.00	1.60	0.64	0.43	0.72
$\Delta_{FS4\ vs.\ NS4}$	0.08	-0.02	-0.11	0.02	-2.40	1.32	-1.06	0.88	0.00	0.00	-0.71	-0.09
NS5	11.15	1.21	8.84	0.95	40.26	2.11	42.88	1.41	1.53	0.72	0.90	0.85
FS5	10.89	1.47	8.90	1.03	40.82	1.99	43.44	1.25	1.55	0.71	1.01	0.84
$\Delta_{FS5\ vs.\ NS5}$	-0.25	0.26	0.05	0.08	0.56	-0.12	0.55	-0.16	0.02	-0.01	0.11	-0.01
NS6	10.47	0.71	8.65	0.78	40.45	2.18	43.20	1.29	1.88	0.12	1.03	0.83
FS6	8.96	0.85	8.56	0.78	35.05	1.60	35.90	1.77	1.88	0.12	0.00	0.00
$\Delta_{FS6\ vs.\ NS6}$	-1.51	0.14	-0.08	0.00	-5.39	-0.58	-7.30	0.49	0.00	0.00	-1.02	-0.83
NW1	9.54	0.88	8.70	0.84	38.07	5.37	41.77	5.12	1.77	0.49	0.33	0.67
FW1	9.35	0.75	8.60	0.78	27.97	1.76	26.87	2.03	1.90	0.13	0.00	0.00
$\Delta_{FW1\ vs.\ NW1}$	-0.20	-0.13	-0.10	-0.06	-10.10	-3.61	-14.90	-3.08	0.13	-0.36	-0.33	-0.67
NW2	9.37	0.73	8.69	0.82	38.85	3.57	42.18	2.57	1.90	0.13	0.84	0.85
FW2	9.53	0.82	8.64	0.81	40.95	2.71	43.52	1.98	1.57	0.72	1.29	0.74
$\Delta_{FW2\ vs.\ NW2}$	0.16	0.08	-0.05	0.00	2.10	-0.86	1.34	-0.59	-0.34	0.60	0.45	-0.11
NW3	9.46	0.72	8.58	0.81	42.01	4.51	45.88	3.51	1.91	0.12	0.70	0.84
FW3	9.52	0.68	8.67	0.78	42.10	4.52	45.97	3.46	1.90	0.13	0.73	0.85
$\Delta_{FW3\ vs.\ NW3}$	0.06	-0.04	0.09	-0.03	0.10	0.01	0.09	-0.05	0.00	0.01	0.03	0.01
NW4	9.62	0.63	8.66	0.74	39.15	3.41	42.41	2.42	1.91	0.11	0.84	0.85
FW4	10.05	0.85	8.75	0.78	38.47	3.59	41.41	2.84	1.55	0.74	0.59	0.81
$\Delta_{FW4\ vs.\ NW4}$	0.43	0.22	0.10	0.04	-0.69	0.18	-1.00	0.43	-0.36	0.63	-0.25	-0.04
NW5	9.51	0.70	8.67	0.78	38.41	3.96	41.89	3.20	1.90	0.11	0.71	0.84
FW5	9.18	0.90	8.61	0.83	38.88	4.15	41.88	3.40	1.79	0.45	0.91	0.85
$\Delta_{FW5\ vs.\ NW5}$	-0.33	0.20	-0.06	0.05	0.46	0.19	-0.01	0.20	-0.11	0.34	0.20	0.02
NW5	9.51	0.70	8.67	0.78	38.41	3.96	41.89	3.20	1.90	0.11	0.71	0.84
FW6	8.39	0.77	8.25	0.79	39.46	6.84	40.39	6.57	1.90	0.12	1.15	0.81
$\Delta_{FW6\ vs.\ NW5}$	-1.12	0.07	-0.42	0.01	1.04	2.88	-1.50	3.37	0.00	0.01	0.44	-0.02

In comparison to the baselines without faults, Tables 9-11 indicate that:

- the fault 1 (i.e., positive offset equal to +3.0 °C for the return air temperature sensor) strongly changes (i) the arithmetic mean of T_{RA}, $T_{A,out,PostHC}$, T_{SA} and $T_{F,out,PostHC}$ during both summer and winter (Tables 9 and 10), (ii) the standard deviation of $T_{A,out,PostHC}$ and T_{SA} during winter (Table 9), (iii) the standard deviation of $T_{F,out,PostHC}$, $T_{F,in,PostHC}$ and $\dot{V}_{F,in,PostHC}$ during winter (Tables 10 and 11), as well as (iv) the arithmetic mean of $T_{F,in,PostHC}$ during winter (Table 10), due to the fact that the measured return air temperature is higher than the real one;
- the occurrence of the fault 2 (i.e., negative offset equal to –3.0 °C for the return air temperature sensor) significantly affects (i) the arithmetic mean of T_{RA}, $T_{A,out,PostHC}$ and T_{SA} during summer (Table 9), as well as (ii) the arithmetic mean of $T_{A,out,PostHC}$ and T_{SA} during winter (Table 9), taking into account that the real return air temperature is greater than the measured one;
- not very significant variations are recognized in the case of the fault 3 (i.e., positive offset equal to +15% for the return air relative humidity sensor) in terms of arithmetic mean and standard deviations of the 16 above-mentioned key operational parameters;

- the fault 4 (i.e., negative offset equal to –15% for the return air relative humidity sensor) greatly modifies (i) the arithmetic mean of $T_{A,out,PostHC}$, T_{SA}, $RH_{A,out,PostHC}$, RH_{SA} and $\dot{V}_{F,in,PostHC}$ during summer (Tables 9-11), as well as (ii) the standard deviation of $\dot{V}_{F,in,CC}$ during winter (Table 11), due to the reason that the real return air relative humidity is larger than the measured one);
- the occurrence of the fault 5 (i.e., complete failure of the return air fan) relevantly changes the arithmetic mean of T_{MA} during winter (Table 9);
- the variations associated to the occurrence of the fault 6 (i.e., complete failure of the supply air fan) are fully relevant in terms of (i) both the arithmetic mean and the standard deviation of both $T_{A,out,PostHC}$ and T_{SA} during both summer and winter (Table 9), (ii) the arithmetic mean of $R_{HA,out,PostHC}$ during winter (Table 10), (iii) the arithmetic mean of $T_{F,out,PostHC}$, $T_{F,in,PostHC}$ and $\dot{V}_{F,in,PostHC}$ during summer (Table 11), (iv) the standard deviation of $\dot{V}_{F,in,PostHC}$ during summer (Table 11), as well as (v) the standard deviation of $T_{F,out,PostHC}$ and $T_{F,in,PostHC}$ during winter (Table 11).

In addition, it should be highlighted that:

- among the largest values of the parameter Δ (Eq. 12) denoted by red font in Table 9, the most significant results are those ones associated to $\Delta_{FW6\ vs.\ NW5}$ for the arithmetic mean of $T_{A,out,PostHC}$ (11.69 °C) and $\Delta_{FW1\ vs.\ NW1}$ for the standard deviation of $T_{A,out,PostHC}$ (–7.49 °C);
- among the largest values of the parameter Δ (Eq. 12) highlighted by red font in Table 10, the most relevant data are those ones associated to $\Delta_{FW4\ vs.\ NW4}$ for the arithmetic mean of RH_{SA} (36.36%) and $\Delta_{FW6\ vs.\ NW5}$ for the standard deviation of $RH_{A,out,PostHC}$ (–17.35%);
- among the largest values of the parameter Δ (Eq. 12) underlined by red font in Table 11, the most important results are those ones associated to $\Delta_{FW1\ vs.\ NW1}$ for the arithmetic mean of $T_{F,in,PostHC}$ (–14.90 °C) and $\Delta_{FW1\ vs.\ NW1}$ for the standard deviation of $T_{F,out,PostHC}$ (–3.61 °C).

Table 12 reports, for each operating variable and faulty scenario, the Symptom Occurrence Probability (SOP) representing the time percentage of the testing period during which the condition specified by Eq. 11 (suggested by [32]) is verified:

$$SOP = FST/OT \tag{13}$$

where FST (Fault Symptom Time) is the time when a fault symptom is observed (based on Eq. 11) in a single faulty test and OP (Operational Time) is the total operational time of the given faulty test.

For each line of Table 12, the green shade has been assigned to the cell corresponding to the lowest value of SOP, while the largest values of SOP have been highlighted by red shades.

In the case of the positive offset of the return air temperature sensor (i.e, fault 1), the occurrence of the symptom is described by the return air temperature during both summer and winter (SOP larger than 98%); during winter the fault 1 strongly affects also the inlet and outlet water temperature of the post-heating coil; during summer, also the relative humidity at the outlet of both the cooling and post-heating coils as well as the mixed air temperature are good descriptors of the fault occurrence.

Similarly, the return air temperature is characterized by very high values of SOP (larger than 93%) also in the case of the negative offset of the return air temperature sensor (i.e, fault 2) during both summer and winter conditions.

The fault 3 (i.e, positive offset of the return air relative humidity sensor) significantly affects the return air relative humidity (SOP = 89.4%) during summer, while during winter the measured parameters are characterized by SOP values not larger than 62.1% (this latter value is assumed by the relative humidity at the outlet of the post-heating coil).

The impact of the fault 4 (i.e, negative offset of the return air relative humidity sensor) is relevant in terms of return air relative humidity during both summer (SOP = 99.8%) and winter (SOP = 100%); the SOP assumes a significant value (SOP = 82.6%) also for the relative humidity of the supply air during summer.

The complete failure of the return air fan (i.e., fault 5) mainly affects both the mixed air temperature and relative humidity during summer (SOP greater than 82%), while during winter the relative humidity at the outlet of the cooling coil (SOP = 81.6%) is the most influenced parameter.

In the case of failure of the supply air fan (i.e., fault 6), the values of SOP are larger than 81% for a number of parameters (RH_{RA}, $RH_{A,out,CC}$, $T_{A,out,PostHC}$, $T_{F,out,CC}$, $\dot{V}_{F,in,PostHC}$, $T_{F,out,PostHC}$ and $T_{F,in,PostHC}$), with SOP = 100% for

RH_{RA} and $\dot{V}_{F,in,PostHC}$; similarly, during winter, the fault 6 is characterized by a significant impact on most of the measured parameters with an average SOP equal to 56.2% (even if it is always lower than 100%, with the maximum value of 92.8% achieved for the parameter $T_{F,out,PostHC}$).

Table 12. Symptom occurrence probability (SOP) as a function of tests and measured parameters.

	FS1 vs. NS1	FS2 vs. NS2	FS3 vs. NS3	FS4 vs. NS4	FS5 vs. NS5	FS6 vs. NS6	FW1 vs. NW1	FW2 vs. NW2	FW3 vs. NW3	FW4 vs. NW4	FW5 vs. NW5	FW6 vs. NW5
$T_{A,out,CC}$	0.7	33.8	0.6	14.1	15.7	37.2	4.5	54.4	4.8	58.6	51.6	78.7
T_{RA}	98.1	100.0	25.5	61.0	37.9	41.1	100.0	93.1	43.2	47.9	40.9	39.2
RH_{RA}	46.6	44.9	89.4	99.8	28.0	100.0	49.5	38.1	39.9	100.0	50.6	14.5
T_{SA}	63.9	67.2	33.1	59.1	56.6	24.0	4.6	65.8	52.3	48.5	64.8	82.1
RH_{SA}	67.9	73.3	52.2	82.6	47.5	3.7	13.0	37.3	56.7	55.4	54.9	78.2
$RH_{A,out,CC}$	80.2	58.6	1.5	3.5	51.6	81.2	57.6	42.9	4.4	41.6	81.6	80.8
T_{MA}	81.5	70.6	29.4	24.7	82.3	19.0	32.4	77.4	11.5	28.1	66.3	49.2
RH_{MA}	24.0	46.1	69.1	76.6	89.8	32.3	51.2	26.5	11.6	69.9	50.3	9.6
$T_{A,out,PostHC}$	65.8	41.7	26.9	40.2	51.6	93.8	0.0	72.8	36.8	54.1	67.3	80.5
$RH_{A,out,PostHC}$	82.0	21.7	61.0	72.8	60.6	2.4	0.0	46.8	62.1	49.3	55.5	74.8
$\dot{V}_{F,in,CC}$	0.4	32.1	0.2	14.2	17.5	0.5	0.5	19.2	0.5	20.5	6.6	0.5
$T_{F,out,CC}$	16.9	32.7	11.4	15.3	33.5	86.7	30.0	38.0	37.8	50.1	45.2	65.1
$T_{F,in,CC}$	23.1	42.5	15.6	31.3	30.3	33.8	36.6	37.1	40.2	41.2	42.8	40.0
$\dot{V}_{F,in,PostHC}$	72.0	14.2	37.6	73.0	39.6	100.0	0.0	73.7	41.4	32.9	52.1	66.5
$T_{F,out,PostHC}$	65.7	29.8	21.5	71.1	30.7	96.1	100.0	30.4	43.3	38.3	34.7	92.8
$T_{F,in,PostHC}$	70.2	33.7	31.8	62.0	30.0	97.5	100.0	20.8	32.2	39.2	21.9	47.1

6. Conclusions

The effects of 6 typical faults of AHUs have been assessed in terms of thermal/hygrometric indoor comfort time and patterns of key operating parameters in order to help building operators and facility engineers in recognizing different fault symptoms and identifying faults of AHUs. The assessment has been performed by contrasting experimental data associated with fault free and faulty tests carried out during Italian summer and winter under similar boundary conditions.

The experimental data highlighted that most adverse fault types in terms of thermal comfort time are the faults F1 (positive offset of the return air temperature sensor equal to +3 °C) and F2 (negative offset of the return air temperature sensor equal to −3 °C) during both summer and winter. With reference to the hygrometric comfort time, the most unfavourable fault type correspond to the fault F4 (negative offset of the return air relative humidity sensor equal to −15%) during both heating and cooling seasons.

The Symptom Occurrence Probability (SOP) values, calculated based on the measured data, underlined that both the fault corresponding to the positive offset (+3 °C) of the return air temperature sensor (F1) and the fault corresponding to the complete failure of the supply air fan (F6) represent the fault types more significantly influencing the most important AHU key operating parameters during both winter and summer.

The relevance of the effects associated to the selected faults are summarized in Tables C.1-C.4 of Appendix C.

The authors will upload the measured data in a public data repository, allowing its utilization for institutional and research purposes to AFDD developers, AFDD users, and research organizations.

The presented experimental database will be extended over time in order to investigate a broader range of boundary conditions, additional severities of the selected faults as well as different types of faults (for example, potential faults associated to the coils' valves and dampers). In addition, the authors will extend the present analysis (where the faults have been introduced at the beginning of the faulty tests and maintained during the entire duration of the experiments) by also considering (i) faults arising suddenly during HVAC operation and remaining at a constant level after the occurrence, as well as (ii) shorter faulty scenarios where a component is 'sticky' and takes more time to be moved/operated with respect to normal operation. In the future, the cases of

multiple faults occurring simultaneously will be also evaluated. Finally, the faults will be also assessed by using novel weighted multi-criteria key performance indicators in terms of energy consumption, GHG emissions and costs. In the future, a dynamic simulation model of the investigated AHU will be developed and validated in contrast with experimental faulty and fault free in order to analyse wider ranges of faulty scenarios. The final aim of the research is the development of an innovative tool for performing AFDD analyses based on supervised data-driven methods customized on the experimental results.

Appendix A

The boundary conditions of the normal tests (baselines) with the corresponding/similar faulty experiments have been compared in the Figures A.1a)-A.1l) from a qualitative point of view in terms of outside air temperature (T_{OA}), outside air relative humidity (RH_{OA}), initial return air temperature ($T_{RA,initial}$) and initial return air relative humidity ($RH_{RA,initial}$). In particular, Figure A.1a) compares the tests NS1 and FS1, Figure A.1b) compares the tests NS2 and FS2, Figure A.1c) compares the tests NS3 and FS3, Figure A.1d) compares the tests NS4 and FS4, Figure A.1e) compares the test NS5 and FS5, Figure A.1f) compares the tests NS6 and FS6, Figure A.1g) compares the tests NW1 and FW1, Figure A.1h) compares the tests NW2 and FW2, Figure A.1i) compares the tests NW3 and FW3, Figure A.1j) compares the tests NW4 and FW4, Figure A.1k) compares the tests NW5 and FW5 and Figure A.1l) compares the tests NW5 and FW6.

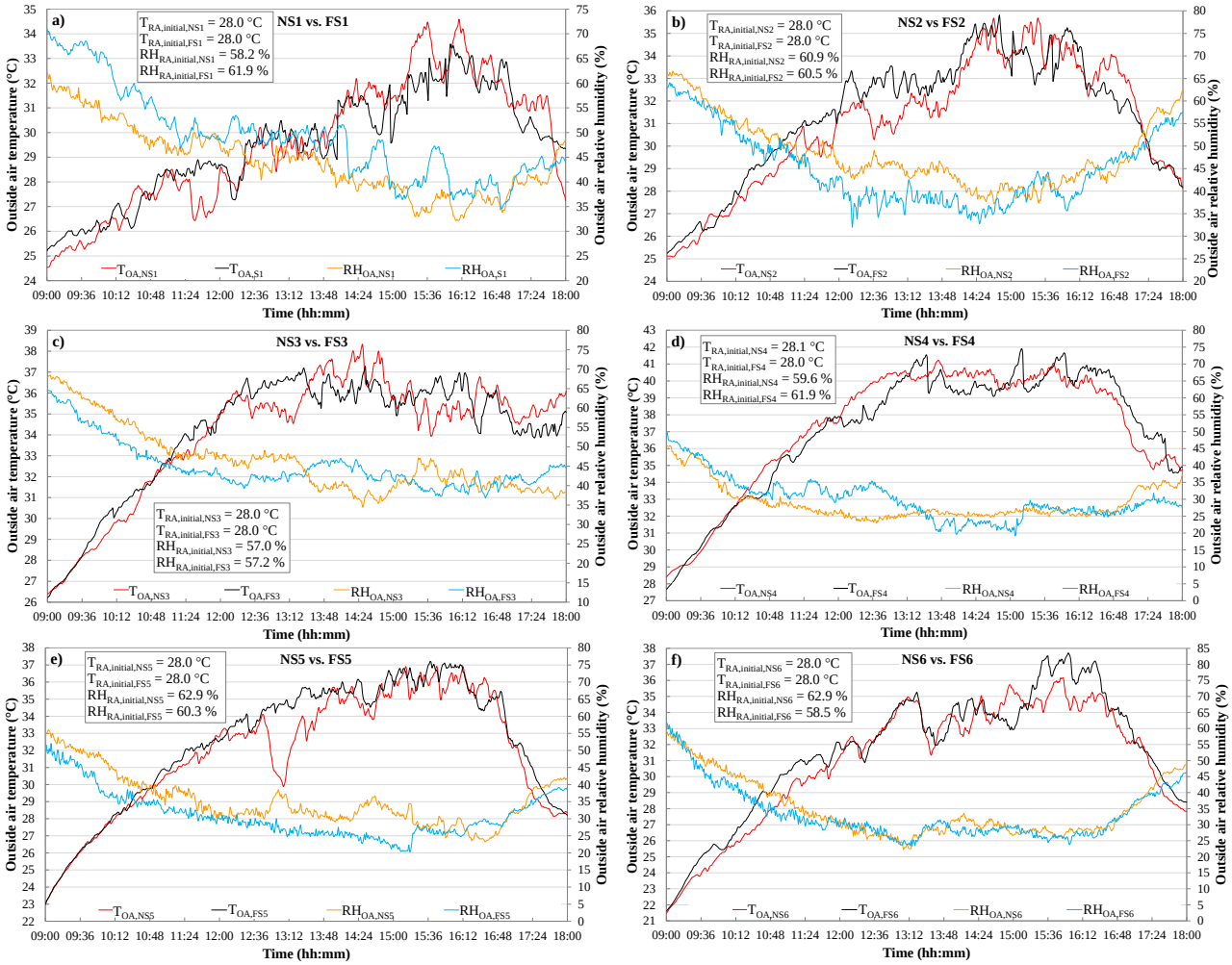

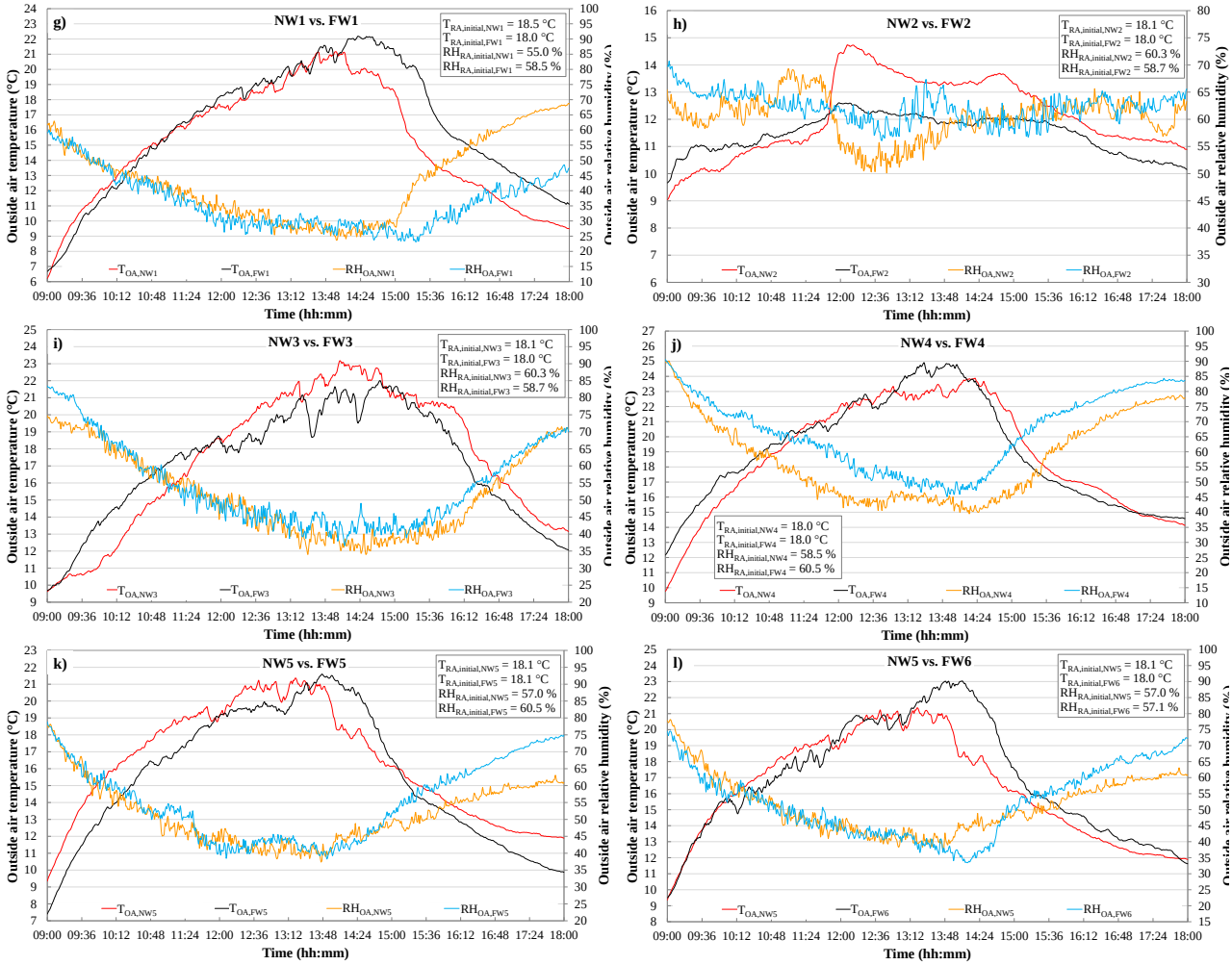

Figure A.1. Comparison of normal and faulty tests in terms of T_{OA}, RH_{OA} and return initial conditions: comparison between NS1 and FS1 (a), NS2 and FS2 (b), NS3 and FS3 (c), NS4 and FS4 (d), NS5 and FS5 (e), NS6 and FS6 (f), NW1 and FW1 (g), NW2 and FW2 (h), NW3 and FW3 (i), NW4 and FW4 (j), NW5 and FW5 (k), NW5 and FW6 (l).

Appendix B

In Figures B.1, B.2 and B.3, the experimental trends of key operating parameters measured during the fault free and faulty tests have been compared; in order to better highlight the results of the comparison, the following parameters/residuals have been calculated according to the experimental data and reported in the above-mentioned figures as a function of the time:

$$\Delta T_{RA} = T_{RA,Baseline} - T_{RA,Faulty} \quad \text{(B.1)}$$

$$\Delta T_{MA} = T_{MA,Baseline} - T_{MA,Faulty} \quad \text{(B.2)}$$

$$\Delta T_{A,out,CC} = T_{A,out,CC,Baseline} - T_{A,out,CC,Faulty} \quad \text{(B.3)}$$

$$\Delta T_{A,out,PostHC} = T_{A,out,PostHC,Baseline} - T_{A,out,PostHC,Faulty} \quad \text{(B.4)}$$

$$\Delta T_{SA} = T_{SA,Baseline} - T_{SA,Faulty} \quad \text{(B.5)}$$

$$\Delta RH_{RA} = RH_{RA,Baseline} - RH_{RA,Faulty} \quad \text{(B.6)}$$

$$\Delta RH_{MA} = RH_{MA,Baseline} - RH_{MA,Faulty} \quad \text{(B.7)}$$

$$\Delta RH_{A,out,CC} = RH_{A,out,CC,Baseline} - RH_{A,out,CC,Faulty} \quad \text{(B.8)}$$

$$\Delta RH_{A,out,PostHC} = RH_{A,out,\ PostHC,Baseline} - RH_{A,out,\ PostHC,Faulty} \quad \text{(B.9)}$$

$$\Delta RH_{SA} = RH_{SA,Baseline} - RH_{SA,Faulty} \quad \text{(B.10)}$$

$$\Delta T_{F,out,CC} = T_{F,out,CC,Baseline} - T_{F,out,CC,Faulty} \quad \text{(B.11)}$$

$$\Delta T_{F,in,CC} = T_{F,in,CC,Baseline} - T_{F,in,CC,Faulty} \quad \text{(B.12)}$$

$$\Delta T_{F,out,PostHC} = T_{F,out,\ PostHC,Baseline} - T_{F,out,\ PostHC,Faulty} \quad \text{(B.13)}$$

$$\Delta T_{F,in,PostHC} = T_{F,in,\ PostHC,Baseline} - T_{F,in,\ PostHC,Faulty} \quad \text{(B.14)}$$

$$\Delta\dot{V}_{F,in,CC} = \dot{V}_{F,in,CC,Baseline} - \dot{V}_{F,in,CC,Faulty} \quad \text{(B.15)}$$

$$\Delta\dot{V}_{F,in,PostHC} = \dot{V}_{F,in,PostHC,Baseline} - \dot{V}_{F,in,PostHC,Faulty} \quad \text{(B.16)}$$

where $T_{RA,Baseline}$, $T_{MA,Baseline}$, $T_{A,out,CC,Baseline}$, $T_{A,out,PostHC,Baseline}$, $T_{SA,Baseline}$, $RH_{RA,Baseline}$, $RH_{MA,Baseline}$, $RH_{A,out,CC,Baseline}$, $RH_{A,out,PostHC,Baseline}$, $RH_{SA,Baseline}$, $T_{F,out,CC,Baseline}$, $T_{F,in,CC,Baseline}$, $T_{F,out,PostHC,Baseline}$, $T_{F,in,PostHC,Baseline}$, $\dot{V}_{F,in,CC,Baseline}$ and $\dot{V}_{F,in,PostHC,Baseline}$ are the values measured during the normal operation (baselines), while $T_{RA,Faulty}$, $T_{MA,Faulty}$, $T_{A,out,CC,Faulty}$, $T_{A,out,PostHC,Faulty}$, $T_{SA,Faulty}$, $RH_{RA,Faulty}$, $RH_{MA,Faulty}$, $RH_{A,out,CC,Faulty}$, $RH_{A,out,PostHC,Faulty}$, $RH_{SA,Faulty}$, $T_{F,out,CC,Faulty}$, $T_{F,in,CC,Faulty}$, $T_{F,out,PostHC,Faulty}$, $T_{F,in,PostHC,Faulty}$, $\dot{V}_{F,in,CC,Faulty}$ and $\dot{V}_{F,in,PostHC,Faulty}$ represent the values measured in the case of fault occurrence. In more detail, Figure B.1 compares the faulty and fault free tests in terms of ΔT_{RA}, ΔT_{MA}, $\Delta T_{A,out,CC}$, $\Delta T_{A,out,PostHC}$ and ΔT_{SA} (Eqs. B.1-B.5); Figure B.2 compares the faulty and fault free tests in terms of ΔRH_{RA}, ΔRH_{MA}, $\Delta RH_{A,out,CC}$, $\Delta RH_{A,out,PostHC}$ and ΔRH_{SA} (Eqs. B.6-B.10); Figure B.3 compares the faulty and fault free tests in terms of $\Delta T_{F,out,CC}$, $\Delta T_{F,in,CC}$, $\Delta T_{F,out,PostHC}$, $\Delta T_{F,in,PostHC}$, $\Delta\dot{V}_{F,in,CC}$ and $\Delta\dot{V}_{F,in,PostHC}$ (Eqs. B.11-B.16). In order to facilitate the readability of the figures and the comparison among them, the same range of values on the vertical axes of all Figures B.1a1)-B.1l1), Figures B.2a2)- B.2l2) and Figures B.3a3)- B.3l3) was adopted.

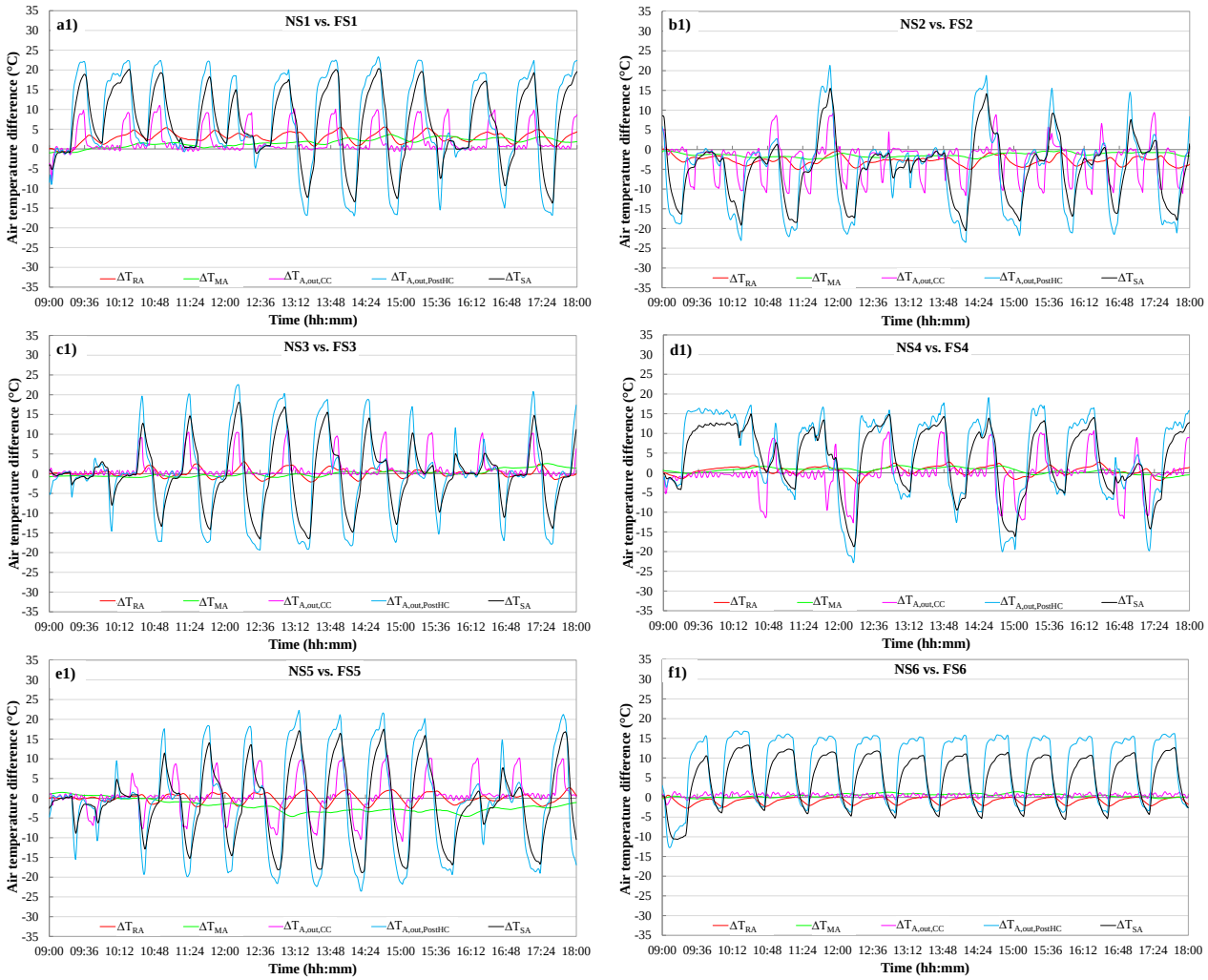

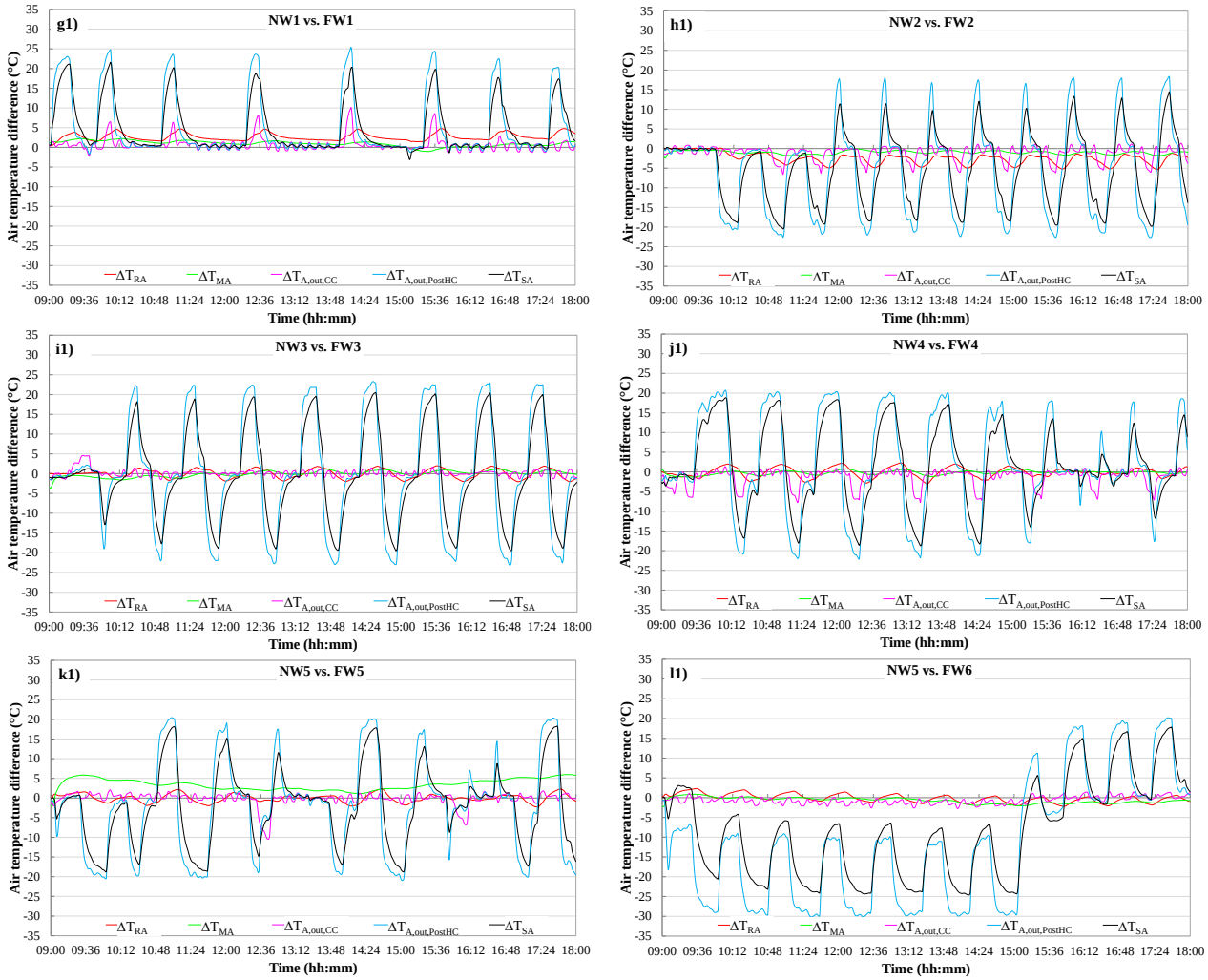

Figure B.1. Comparison of faulty and fault free tests in terms of ΔT_{RA}, ΔT_{MA}, $\Delta T_{A,out,CC}$, $\Delta T_{A,out,PostHC}$ and ΔT_{SA} (Eqs. B.1-B.5): comparison between NS1 and FS1 (a1), NS2 and FS2 (b1), NS3 and FS3 (c1), NS4 and FS4 (d1), NS5 and FS5 (e1), NS6 and FS6 (f1), NW1 and FW1 (g1), NW2 and FW2 (h1), NW3 and FW3 (i1), NW4 and FW4 (j1), NW5 and FW5 (k1), NW5 and FW6 (l1).

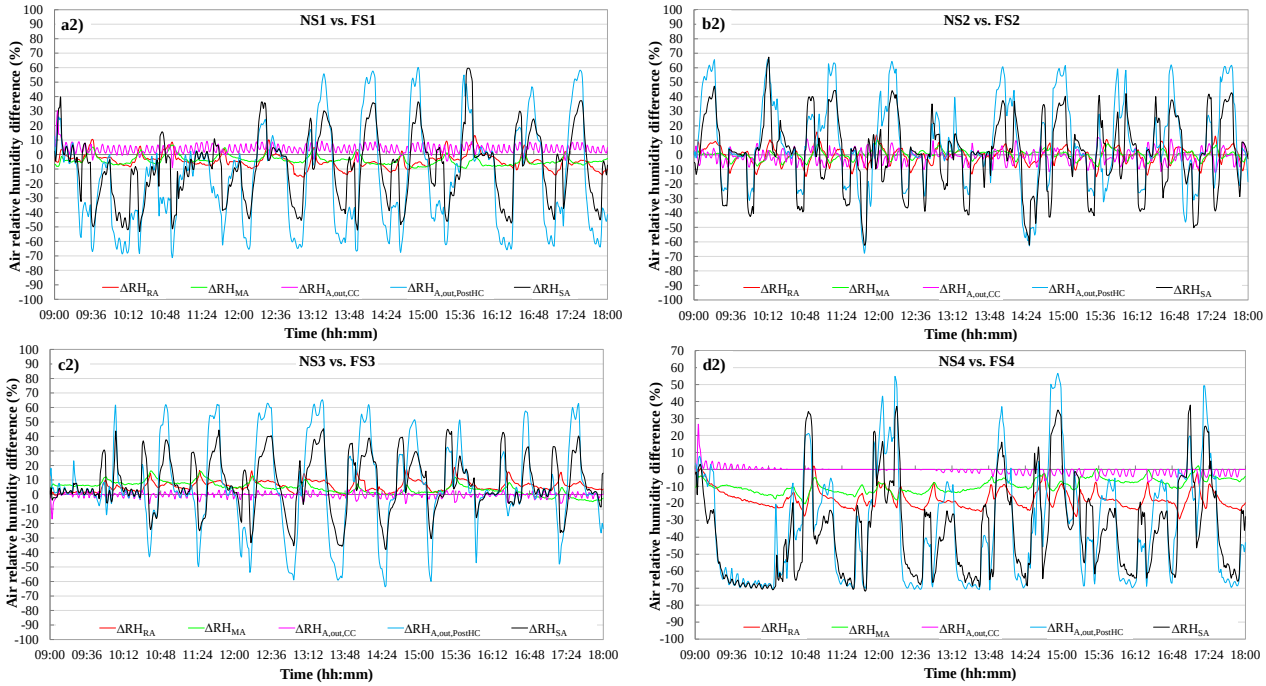

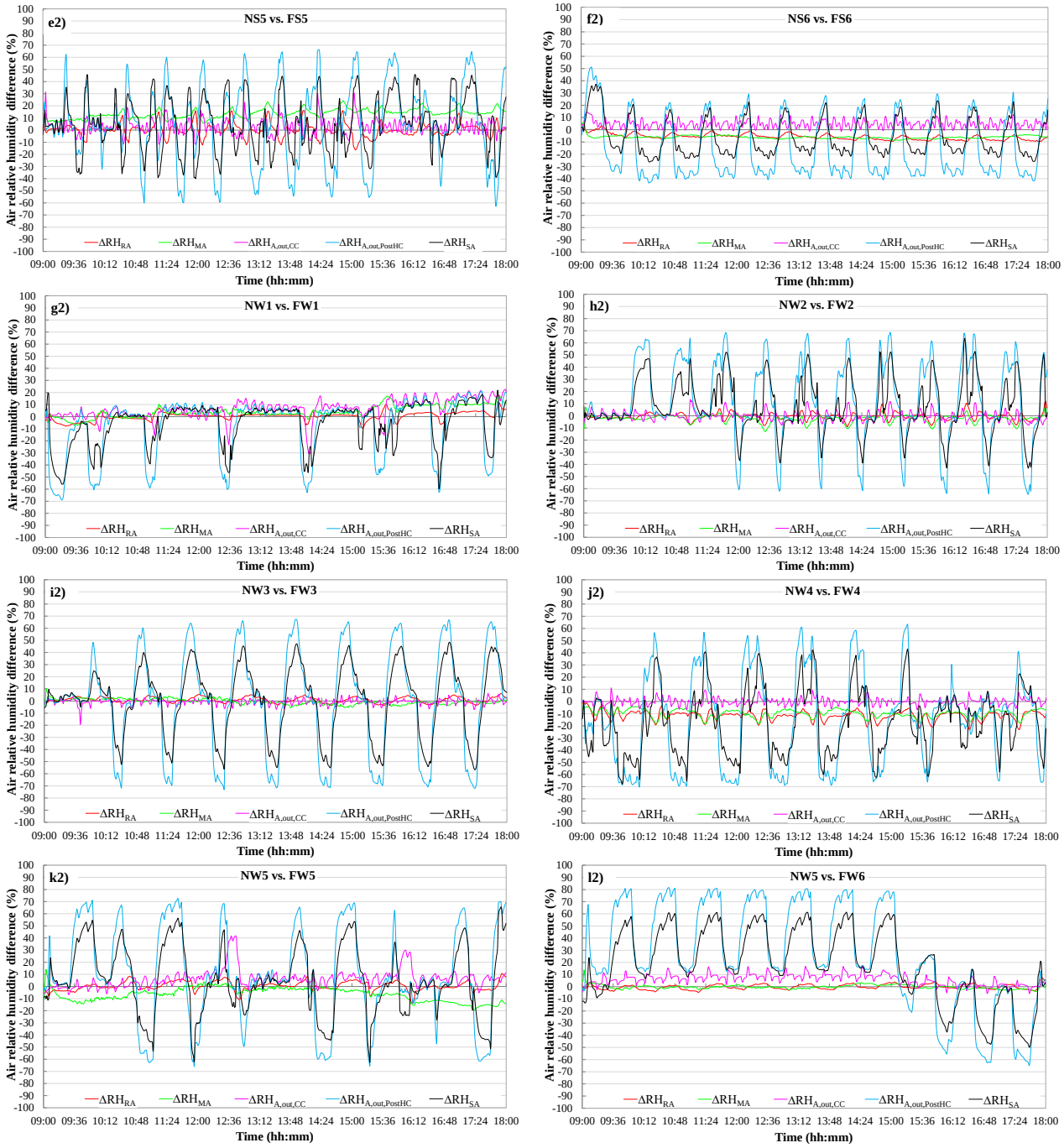

Figure B.2. Comparison of faulty and fault free tests in terms of ΔRH_{RA}, ΔRH_{MA}, $\Delta RH_{A,out,CC}$, $\Delta RH_{A,out,PostHC}$ and ΔRH_{SA} (Eqs. B.6-B.10): comparison between NS1 and FS1 (a2), NS2 and FS2 (b2), NS3 and FS3 (c2), NS4 and FS4 (d2), NS5 and FS5 (e2), NS6 and FS6 (f2), NW1 and FW1 (g2), NW2 and FW2 (h2), NW3 and FW3 (i2), NW4 and FW4 (j2), NW5 and FW5 (k2), NW5 and FW6 (l2).

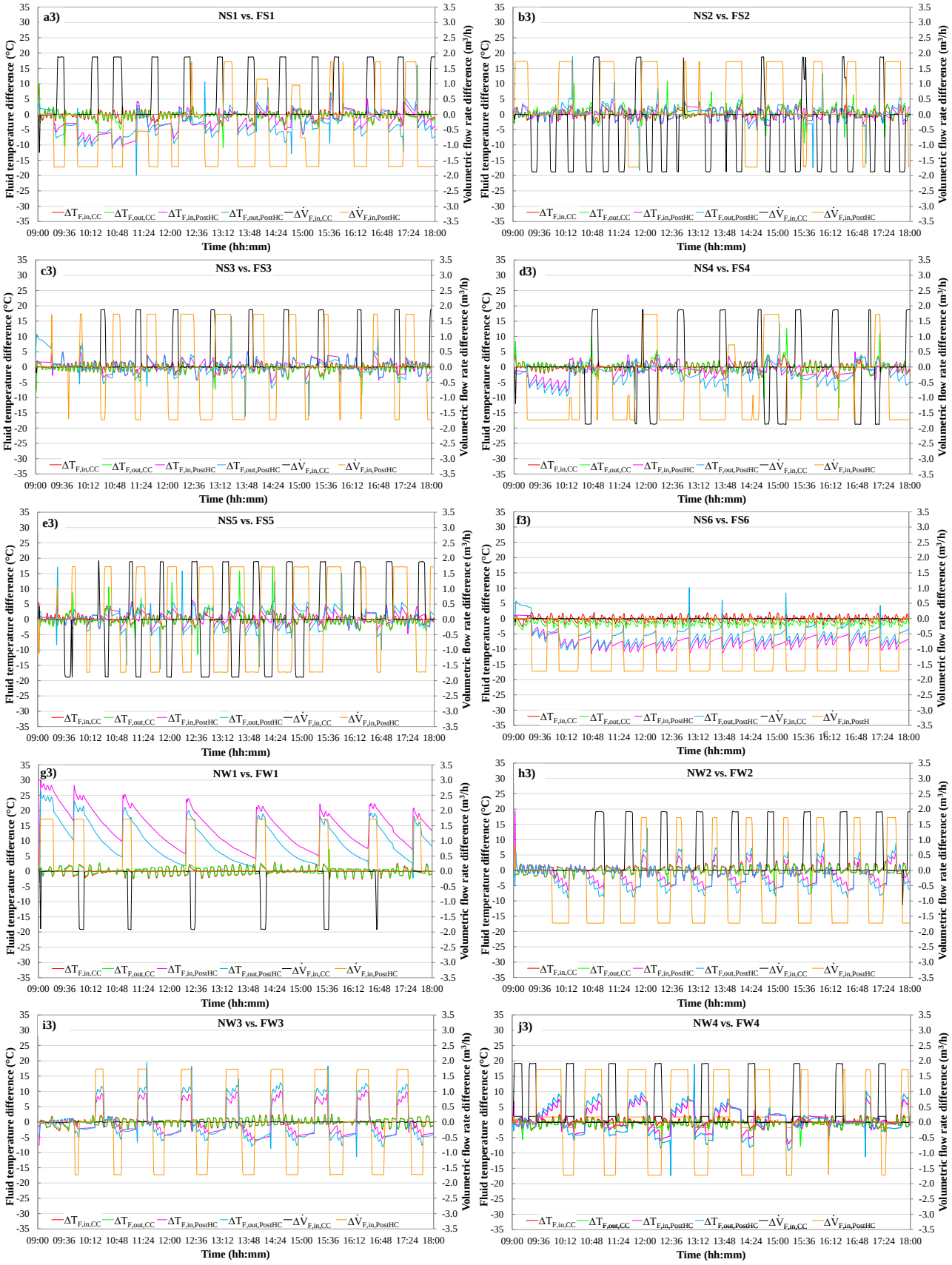
a3)
NS1 vs. FS1
b3)
NS2 vs. FS2
c3)
NS3 vs. FS3
d3)
NS4 vs. FS4
e3)
NS5 vs. FS5
f3)
NS6 vs. FS6
g3)
NW1 vs. FW1
h3)
NW2 vs. FW2
i3)
NW3 vs. FW3
j3)
NW4 vs. FW4
Fluid temperature difference (°C)
Volumetric flow rate difference (m³/h)
Time (hh:mm)
09:00 09:36 10:12 10:48 11:24 12:00 12:36 13:12 13:48 14:24 15:00 15:36 16:12 16:48 17:24 18:00
ΔT_F,in,CC
ΔT_F,out,CC
ΔT_F,in,PostHC
ΔT_F,out,PostHC
ΔV̇_F,in,CC
ΔV̇_F,in,PostHC

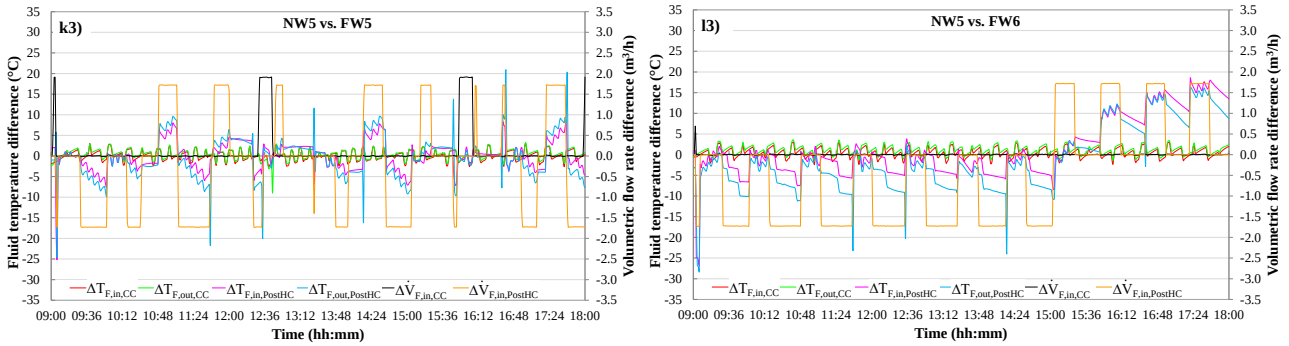

Figure B.3. Comparison of faulty and fault free tests in terms of $\Delta T_{F,out,CC}$, $\Delta T_{F,in,CC}$, $\Delta T_{F,out,PostHC}$, $\Delta T_{F,in,PostHC}$, $\Delta \dot{V}_{F,in,CC}$ and $\Delta \dot{V}_{F,in,PostHC}$ (Eqs. B.11-B.16): comparison between NS1 and FS1 (a3), NS2 and FS2 (b3), NS3 and FS3 (c3), NS4 and FS4 (d3), NS5 and FS5 (e3), NS6 and FS6 (f3), NW1 and FW1 (g3), NW2 and FW2 (h3), NW3 and FW3 (i3), NW4 and FW4 (j3), NW5 and FW5 (k3), NW5 and FW6 (l3).

Appendix C

The relevance of the effects associated with the selected faults are summarized in Tables C.1-C.4 of this Appendix, where one of the following signs has been assigned according to the values assumed by the parameters $\%DCT_T$ (Eq. 7), $\%DCT_{RH}$ (Eq. 8) and Δ (Eq. 12):

- "0" indicates that the fault causes not substantial changes;
- "+" indicates that the fault causes slightly positive changes;
- "+ +" indicates that the fault causes substantial positive changes;
- "–" indicates that the fault causes slightly negative changes;
- "– –" indicates that the fault causes substantial negative changes.

In particular, Tables C.1-C.4 report, respectively, the symptoms' relevance (specified in the associated legends) of the selected faults in terms of thermal/hygrometric comfort time, air temperature, air relative humidity and heat carrier fluid properties with the aim of facilitating the readability of the experimental outcomes. A different coloured shade is also assigned to each condition in Tables C.1-C.4 according to the corresponding legends.

Table C.1. Symptoms' relevance of the selected faults in terms of thermal/hygrometric comfort time.

Faulty test	Thermal comfort time	Hygrometric comfort time
FS1	– –	– –
FS2	– –	–
FS3	0	– –
FS4	–	– –
FS5	0	0
FS6	–	– –
FW1	– –	0
FW2	– –	0
FW3	0	0
FW4	0	– –
FW5	0	0
FW6	0	0
Legend		
0	$-10\% \leq \%DCT_T \leq +10\%$ $-10\% \leq \%DCT_{RH} \leq +10\%$	
+	$+10\% < \%DCT_T \leq +20\%$ $+10\% < \%DCT_{RH} \leq +20\%$	
+ +	$\%DCT_T > +20\%$ $\%DCT_{RH} > +20\%$	
–	$-20\% \leq \%DCT_T < -10\%$ $-20\% \leq \%DCT_{RH} < -10\%$	
– –	$\%DCT_T < -20\%$ $\%DCT_{RH} < -20\%$	

Table C.2. Symptoms' relevance of the selected faults in terms of air temperature.

Faulty test	T_{RA}		T_{MA}		$T_{A,out,CC}$		$T_{A,out,PostHC}$		T_{SA}	
	μ	**σ**	**μ**	**σ**	**μ**	**σ**	**μ**	**σ**	**μ**	**σ**
FS1	– –	0	–	0	–	–	– –	0	– –	0
FS2	+ +	0	0	0	+	+	+ +	–	+ +	–
FS3	0	0	0	0	0	–	0	0	0	0
FS4	0	0	0	0	0	0	– –	–	– –	0
FS5	0	0	+	0	0	0	0	0	0	0
FS6	0	0	0	0	0	0	– –	– –	– –	– –
FW1	– –	0	0	0	0	0	– –	– –	– –	– –
FW2	+	0	0	0	0	0	+ +	0	+ +	0
FW3	0	0	0	0	0	0	0	0	0	0
FW4	0	0	0	0	0	+	–	0	–	0
FW5	0	0	– –	0	0	0	+	0	+	0
FW6	0	0	0	0	0	0	+ +	+ +	+ +	+ +
Legend										
0	$-1.5\ °C \leq \Delta \leq +1.5\ °C$									
+	$+1.5\ °C < \Delta \leq +2.5\ °C$									
+ +	$\Delta > +2.5\ °C$									
–	$-2.5\ °C \leq \Delta < -1.5\ °C$									
– –	$\Delta < -2.5\ °C$									

Table C.3. Symptoms' relevance of the selected faults in terms of air relative humidity.

Faulty test	RH_{RA}		RH_{MA}		$RH_{A,out,CC}$		$RH_{A,out,PostHC}$		RH_{SA}	
	μ	σ	μ	σ	μ	σ	μ	σ	μ	σ
FS1	0	0	0	0	0	0	+	0	0	0
FS2	0	0	0	0	0	0	0	0	0	0
FS3	0	0	0	0	0	0	0	0	0	0
FS4	+	0	0	0	0	0	+ +	0	+ +	0
FS5	0	0	–	0	0	0	0	0	0	0
FS6	0	0	0	0	0	0	+	–	0	0
FW1	0	0	0	0	0	0	0	–	0	0
FW2	0	0	0	0	0	0	–	0	0	0
FW3	0	0	0	0	0	0	0	0	0	0
FW4	+	0	0	0	0	0	+	0	+	0
FW5	0	0	0	0	0	0	0	0	0	0
FW6	0	0	0	0	0	0	– –	0	–	0

Legend	
0	$-10\% \leq \Delta \leq +10\%$
+	$+10\% < \Delta \leq +20\%$
+ +	$\Delta > +20\%$
–	$-20\% \leq \Delta < -10\%$
– –	$\Delta < -20\%$

Table C.4. Symptoms' relevance of the selected faults in terms of heat carrier fluid parameters.

Faulty test	$T_{F,out,CC}$		$T_{F,in,CC}$		$T_{F,out,PostHC}$		$T_{F,in,PostHC}$		$\dot{V}_{F,in,CC}$		$\dot{V}_{F,in,PostHC}$	
	μ	σ	μ	σ	μ	σ	μ	σ	μ	σ	μ	σ
FS1	0	0	0	0	– –	0	–	0	+	– –	–	0
FS2	0	0	0	0	0	0	0	0	–	+	+	0
FS3	0	0	0	0	0	0	0	0	0	–	0	0
FS4	0	0	0	0	–	0	0	0	0	0	– –	0
FS5	0	0	0	0	0	0	0	0	0	0	0	0
FS6	–	0	0	0	– –	0	– –	0	0	0	– –	– –
FW1	0	0	0	0	– –	– –	– –	– –	0	–	–	– –
FW2	0	0	0	0	+	0	0	0	–	+	+	0
FW3	0	0	0	0	0	0	0	0	0	0	0	0
FW4	0	0	0	0	0	0	0	0	–	+ +	0	0
FW5	0	0	0	0	0	0	0	0	0	+	0	0
FW6	0	0	0	0	0	+ +	–	+ +	0	0	+	0

Legend	
0	$-1.5\ °C \leq \Delta \leq +1.5\ °C$ $0.3\ m^3/h \leq \Delta \leq +0.3\ m^3/h$
+	$+1.5\ °C < \Delta \leq +2.5\ °C$ $+0.3\ m^3/h < \Delta \leq +0.6\ m^3/h$
+ +	$\Delta > +2.5\ °C$ $\Delta > +0.6\ m^3/h$
–	$-2.5\ °C \leq \Delta < -1.5\ °C$ $-0.6\ m^3/h \leq \Delta < -0.3\ m^3/h$
– –	$\Delta < -2.5\ °C$ $\Delta < -0.6\ m^3/h$

Nomenclature

Latin letters

AFDD	Automatic fault detection and diagnosis
AHU	Air-Handling Unit
CC	Cooling coil
COP	Coefficient of performance

CT	Cold tank
$CT_{Baseline}$	Comfort time of experimental normal tests
CT_{Faulty}	Comfort time of experimental faulty tests
DB_{RH}	Deadband of $RH_{SP,Room}$ (%)
DB_{T}	Deadband of $T_{SP,Room}$ (°C)
D_{EA}	Exhaust air damper
D_{OA}	Outside air damper
D_{HRS}	Damper of the heat recovery system
D_{RA}	Return air damper
EA	Exhaust air
EER	Energy efficiency ratio
$EXP_{OA,Baseline,i}$	Experimental value of T_{OA} at time step i under healthy conditions (°C)
$EXP_{OA,Faulty,i}$	Experimental value of T_{OA} at time step i under faulty conditions (°C)
FS1	Faulty test with positive offset (+3 °C) of the return air temperature sensor during summer
FS2	Faulty test with negative offset (–3 °C) of the return air temperature sensor during summer
FS3	Faulty test with positive offset (+15%) of the return air relative humidity sensor during summer
FS4	Faulty test with negative offset (–15%) of the return air relative humidity sensor during summer
FS5	Faulty test with complete failure of the return air fan during summer
FS6	Faulty test with complete failure of the supply air fan during summer
FST	Fault Symptom Time (min)
FW1	Faulty test with positive offset (+3 °C) of the return air temperature sensor during winter
FW2	Faulty test with negative offset (–3 °C) of the return air temperature sensor during winter
FW3	Faulty test with positive offset (+15%) of the return air relative humidity sensor during winter
FW4	Faulty test with negative offset (–15%) of the return air relative humidity sensor during winter
FW5	Faulty test with complete failure of the return air fan during winter
FW6	Faulty test with complete failure of the supply air fan during winter
GHG	Greenhouse gas
HP	Heat pump
HRS	Static cross-flow heat recovery system
HT	Hot tank
HUM	Humidifier
HVAC	Heating, ventilation and air-conditioning
LDB_{RH}	Lower deadband of indoor air relative humidity (%)
LDB_{T}	Lower deadband of indoor air temperature (°C)
N	Number of experimental data points
NS1	Normal summer test n°1
NS2	Normal summer test n°2
NS3	Normal summer test n°3
NS4	Normal summer test n°4
NS5	Normal summer test n°5
NS6	Normal summer test n°6
NW1	Normal winter test n°1
NW2	Normal winter test n°2
NW3	Normal winter test n°3
NW4	Normal winter test n°4
NW5	Normal winter test n°5
$N_{out,DBT}$	Number of experimental data points with T_{RA} out of the corresponding deadband
$N_{out,DBRH}$	Number of experimental data points with RH_{RA} out of the corresponding deadband

OAD	Outside air duct
OAFil	Outside air filter
OL_{RAF}	Velocity of the return air fan (%)
OL_{SAF}	Velocity of the supply air fan (%)
OP	Operational Time of a faulty test (min)
OP_{DEA}	Opening percentage of the D_{EA} (%)
OP_{DHRS}	Opening percentage of the D_{HRS} (%)
OP_{DOA}	Opening percentage of the D_{OA} (%)
OP_{DRA}	Opening percentage of the D_{RA} (%)
OP_{V_CC}	Opening percentage of valve regulating the flow entering the CC (%)
OP_{V_HUM}	Opening percentage of valve regulating the flow exiting the HUM (%)
OP_{V_PostHC}	Opening percentage of valve regulating the flow entering the PostHC (%)
OP_{V_PreHC}	Opening percentage of valve regulating the flow entering the PreHC (%)
PID	Proportional-integral-derivative
PostHC	Post-heating coil
PreHC	Pre-heating coil
RAD	Return air duct
RAF	Return air fan
RAFil	Return air filter
RAV	Return air vent
$RH_{A,out,CC}$	Cooling coil outlet air relative humidity (%)
$RH_{A,out,CC,Baseline}$	Measured Cooling coil outlet air relative humidity under healthy conditions (%)
$RH_{A,out,CC,Faulty}$	Measured Cooling coil outlet air relative humidity under faulty conditions (%)
$RH_{A,out,PostHC}$	Post-heating coil outlet air relative humidity (%)
$RH_{A,out,PostHC,Baseline}$	Measured post-heating coil outlet air relative humidity under healthy conditions (%)
$RH_{A,out,PostHC,Faulty}$	Measured post-heating coil outlet air relative humidity under faulty conditions (%)
RH_{MA}	Mixed air relative humidity (%)
$RH_{MA,Baseline}$	Measured mixed air relative humidity under healthy conditions (%)
$RH_{MA,Faulty}$	Measured mixed air relative humidity under faulty conditions (%)
RH_{OA}	Outside air relative humidity (%)
RH_{RA}	Return air relative humidity (%)
$RH_{RA,initial}$	Initial indoor return air relative humidity (%)
$RH_{RA,Baseline}$	Measured return air relative humidity under healthy conditions (%)
$RH_{RA,Faulty}$	Measured return air relative humidity under faulty conditions (%)
RH_{Room}	Air relative humidity inside the integrated test room (%)
RH_{SA}	Supply air relative humidity (%)
$RH_{SA,Baseline}$	Measured supply air relative humidity under healthy conditions (%)
$RH_{SA,Faulty}$	Measured supply air relative humidity under faulty conditions (%)
$RH_{SP,Room}$	Desired target of indoor air relative humidity (%)
RMSD	Root mean square difference (°C/%)
RS	Refrigerating system
SAD	Supply air duct
SAF	Supply air fan
SAFil	Supply air filter
SAV	Supply air vent
SOP	Symptom Occurrence Probability (%)
$T_{A,out,CC}$	Air temperature at the outlet of the cooling coil (°C)
$T_{A,out,CC,Baseline}$	Measured air temperature at the outlet of the cooling coil under healthy conditions (°C)
$T_{A,out,CC,Faulty}$	Measured air temperature at the outlet of the cooling coil under faulty conditions (°C)
$T_{A,out,PostHC}$	Air temperature at the outlet of the post-heating coil (°C)
$T_{A,out,PostHC,Baseline}$	Measured air temperature at the outlet of the post-heating coil under healthy conditions (°C)
$T_{A,out,PostHC,Faulty}$	Measured air temperature at the outlet of the post-heating coil under faulty conditions (°C)
T_{CT}	Heat carrier fluid temperature inside the cold tank (°C)
$T_{CT,set\text{-}point}$	Target temperature of heat carrier fluid temperature inside the cold tank (°C)

$T_{F,in,CC}$	Heat carrier fluid temperature at cooling coil inlet (°C)
$T_{F,in,HP}$	Heat carrier fluid temperature at heat pump outlet (°C)
$T_{F,in,PostHC}$	Heat carrier fluid temperature at post-heating coil inlet (°C)
$T_{F,in,PreHC}$	Heat carrier fluid temperature at pre-heating coil inlet (°C)
$T_{F,in,RS}$	Heat carrier fluid temperature at refrigerating system inlet (°C)
$T_{F,out,CC}$	Heat carrier fluid temperature at cooling coil outlet (°C)
$T_{F,out,HP}$	Heat carrier fluid temperature at heat pump outlet (°C)
$T_{F,out,PostHC}$	Heat carrier fluid temperature at post-heating coil outlet (°C)
$T_{F,out,PreHC}$	Heat carrier fluid temperature at pre-heating coil outlet (°C)
$T_{F,out,RS}$	Heat carrier fluid temperature at refrigerating system outlet (°C)
T_{HT}	Heat carrier fluid temperature inside the hot tank (°C)
$T_{HT,set-point}$	Target temperature of heat carrier fluid temperature inside the hot tank (°C)
T_{MA}	Mixed air temperature (°C)
$T_{MA,Baseline}$	Measured mixed air temperature under healthy conditions (°C)
$T_{MA,Faulty}$	Measured mixed air temperature under faulty conditions (°C)
T_{OA}	Outside air temperature (°C)
T_{RA}	Return air temperature (°C)
$T_{RA,initial}$	Initial return air temperature (°C)
$T_{RA,Baseline}$	Measured return air temperature under healthy conditions (°C)
$T_{RA,Faulty}$	Measured return air temperature under faulty conditions (°C)
T_{Room}	Air temperature inside the integrated test room (°C)
T_{SA}	Supply air temperature (°C)
$T_{SA,Baseline}$	Measured supply air temperature under healthy conditions (°C)
$T_{SA,Faulty}$	Measured supply air temperature under faulty conditions (°C)
$T_{SP,Room}$	Desired target of indoor air temperature (°C)
UDB_{RH}	Upper deadband of indoor air relative humidity (%)
UDB_{T}	Upper deadband of indoor air temperature (°C)
VAV	Variable air volume
V_{CC}	Three-way valves supply the cooling coil
V_{HUM}	Three-way valve supply the humidifier
V_{PostHC}	Three-way valve supply the post-heating coil
V_{PreHC}	Three-way valve supply the pre-heating coil
$\dot{V}_{F,in,CC}$	Volumetric flow rate of cooling coil heat carrier fluid (m^3/h)
$\dot{V}_{F,in,PostHC}$	Volumetric flow rate of post-heating coil heat carrier fluid (m^3/h)
$\dot{V}_{F,in,PreHC}$	Volumetric flow rate of pre-heating coil heat carrier fluid (m^3/h)
$X_{Baseline}$	Arithmetic mean μ or standard deviation σ calculated based on the measured values under normal conditions
X_{Faulty}	Arithmetic mean μ or standard deviation σ calculated based on the measured values under faulty conditions
$\Delta RH_{A,out,CC}$	Instantaneous difference in terms of $RH_{A,out,CC}$ between the values measured under healthy and faulty conditions (%)
$\Delta RH_{A,out,PostHC}$	Instantaneous difference in terms of $RH_{A,out,PostHC}$ between the values measured under healthy and faulty conditions (%)
ΔRH_{MA}	Instantaneous difference in terms of RH_{MA} between the values measured under healthy and faulty conditions (%)
$\Delta RH_{out,DBT}$	Difference between RH_{RA} and UDB_{RH} calculated in the case of RH_{RA} is larger than UDB_{RH}, or the difference between LDB_{RH} and RH_{RA} in the case of RH_{RA} is lower than LDB_{RH}
ΔRH_{RA}	Instantaneous difference in terms of RH_{RA} between the values measured under healthy and faulty conditions (%)
ΔRH_{SA}	Instantaneous difference in terms of RH_{SA} between the values measured under healthy and faulty conditions (%)
$\Delta T_{A,out,CC}$	Instantaneous difference in terms of $T_{A,out,CC}$ between the values measured under healthy and faulty conditions (°C)

$\Delta T_{A,out,PostHC}$	Instantaneous difference in terms of $T_{A,out,PostHC}$ between the values measured under healthy and faulty conditions (°C)
$\Delta T_{F,in,CC}$	Instantaneous difference in terms of $T_{F,in,CC}$ between the values measured under healthy and faulty conditions (°C)
$\Delta T_{F,in,PostHC}$	Instantaneous difference in terms of $T_{F,in,PostHC}$ between the values measured under healthy and faulty conditions (°C)
$\Delta T_{F,out,CC}$	Instantaneous difference in terms of $T_{F,out,CC}$ between the values measured under healthy and faulty conditions (°C)
$\Delta T_{F,out,PostHC}$	Instantaneous difference in terms of $T_{F,out,PostHC}$ between the values measured under healthy and faulty conditions (°C)
$\Delta T_{out,DBRH}$	Difference between RH_{RA} and UDB_{RH} calculated in the case of RH_{RA} is larger than UDB_{RH}, or the difference between LDB_{RH} and RH_{RA} in the case of RH_{RA} is lower than LDB_{RH}
$\Delta T_{out,DBT}$	Difference between T_{RA} and UDB_T calculated in the case of T_{RA} is larger than UDB_T, or the difference between LDB_T and T_{RA} in the case of T_{RA} is lower than LDB_T
ΔT_{MA}	Instantaneous difference in terms of T_{MA} between the values measured under healthy and faulty conditions (°C)
ΔT_{RA}	Instantaneous difference in terms of T_{RA} between the values measured under healthy and faulty conditions (°C)
ΔT_{SA}	Instantaneous difference in terms of T_{SA} between the values measured under healthy and faulty conditions (°C)
$\Delta \dot{V}_{F,in,CC}$	Instantaneous difference in terms of $\dot{V}_{F,in,CC}$ between the values measured under healthy and faulty conditions (m^3/h)
$\Delta \dot{V}_{F,in,PostHC}$	Instantaneous difference in terms of $\dot{V}_{F,in,PostHC}$ between the values measured under healthy and faulty conditions (m^3/h)
$\%DCT_T$	Percentage difference in terms of thermal comfort time (%)
$\%DCT_T$	Percentage difference in terms of hygrometric comfort time (%)
$\%V_{Glycol,PreHC}$	Percentage by volume of glycol in the heat carrier fluid entering the PreHC
$\%V_{Glycol,CC}$	Percentage by volume of glycol in the heat carrier fluid entering the CC
$\%V_{Glycol,PostHC}$	Percentage by volume of glycol in the heat carrier fluid entering the PostHC
Greeks	
Δ	Difference between experimental faulty and normal measured values
ε_i	Instantaneous difference (°C/%)
$\overline{\varepsilon}$	Average error (°C/%)
$\left\|\overline{\varepsilon}\right\|$	Absolute average error (°C/%)
$\left\|\overline{\varepsilon}_{T,D}\right\|$	Intensity of thermal discomfort time (°C)
$\left\|\overline{\varepsilon}_{RH,D}\right\|$	Intensity of hygrometric discomfort time (%)
μ	Arithmetic mean (°C/%)
σ	Standard deviation (°C/%)

Acknowledgments

This work was undertaken as part of the program "PON FSE-FESR Ricerca e Innovazione 2014–2020" of the Italian Ministry of Education, University and Research, Action I.1 "Dottorati innovativi con caratterizzazione industriale".

The authors would like to thank the company Belimo (https://www.belimo.com/) for supporting the research activities described in this paper by means of its energy valves.

References

[1] 2021 Global Status Report for Buildings and Construction. Towards a Zero-emission, Efficient and Resilient Buildings and Construction Sector. Available online: https://globalabc.org/sites/default/files/2021-10/GABC_Buildings-GSR-2021_BOOK.pdf (accessed on 1 August 2022).

[2] X. Cao, X. Dai, J. Liu, Building energy-consumption status worldwide and the state-of-the-art technologies for zero-energy buildings during the past decade, Energy Build. 128 (2016).
[3] M. S. Mirnaghi, F. Haghighat, Fault detection and diagnosis of large-scale HVAC systems in buildings using data-driven methods: A comprehensive review, Energy and Buildings 229 (2020) 110492.
[4] W.S. Yun, W.H. Hong, H. Seo, A data-driven fault detection and diagnosis scheme for air handling units in building HVAC systems considering undefined states, Journal of Building Engineering 35 (2021) 102111.
[5] J. Proctor, 2004, "Residential and Small Commercial Central Air Conditioning; Rated Efficiency isn't Automatic," Presentation at the Public Session. ASHRAE Winter Meeting, January 26, Anaheim, CA.
[6] T.M. Rossi, 2004, "Unitary Air Conditioner Field Performance," International Refrigeration and Air Conditioning Conference at Purdue, Paper No. R146, July 12-15, West Lafayette, IN.
[7] Y. Yu, D. Woradechjumroen, D. Yu, A review of fault detection and diagnosis methodologies on air-handling units, Energy and Buildings 82 (2014) 550-562.
[8] M. Liu, D.E. Claridge, W.D. Turner, Continuous commissioning SM of building energy system, ASME J. Solar Energy Eng. 125 (3) (2003) 275-281.
[9] H. Wang, Y. Chen, A robust fault detection and diagnosis strategy for multiple faults of VAV air handling units, Energy and Buildings 127 (2016) 442-451.
[10] S. Deshmukh, S. Samouhos, L. Glicksman, L. Norford, Fault detection in commercial building VAV AHU: A case study of an academic building, Energy Build. 201 (2019) 163-173.
[11] D. D'Urso, A. Sinatra, L. Compagno, F. Chiacchio, Assessment of the optimal preventive maintenance period using stochastic hybrid modelling, 3rd International Conference on Industry 4.0 and Smart Manufacturing, Procedia Computer Science 200 (2022) 1664-1673.
[12] M.R. Sanzana, T. Maul, J.Y. Wong, M.O.M. Abdulrazic, C.-C. Yip, Application of deep learning in facility management and maintenance for heating, ventilation, and air conditioning, Automation in Construction 141 (2022) 104445.
[13] IEA Annex 25, Real time simulation of HVAC system for building optimization, fault detection and diagnosis, ed. Hyvarien J., Karki S., Techical Research Centre of Finland 1996.
[14] IEA Annex 34, Demonstrating automated fault detection and diagnosis methods in real buildings, ed. Dexter A., Technical Research Centre of Finland 2001.
[15] F. Guarino, V. Filomena, L. Maffei, S. Sibilio, A. Rosato, A Review of Fault Detection and Diagnosis Methodologies for Air-Handling Units, Global Journal of Energy Technology Research Updates 6 (2019).
[16] C.P. Au-Yong, A.S. Ali, F. Ahmad, Improving occupants' satisfaction with effective maintenance management of HVAC system in office buildings. Autom. Constr. 43 (2014) 31-37.
[17] S. Frank, G. Lin, X. Jin, R. Singla, A. Farthing, J. Granderson, A performance evaluation framework for building fault detection and diagnosis algorithms, Energy & Buildings 192 (2019) 84-92.
[18] M.S. Piscitelli, D.M. Mazzarelli, A. Capozzoli, Enhancing operational performance of AHUs through an advanced fault detection and diagnosis process based on temporal association and decision rules, Energy Build. 226 (2020) 110369.
[19] G. Lin, H. Kramer, J. Granderson, Building fault detection and diagnostics: Achieved savings, and methods to evaluate algorithm performance, Building and Environment 168 (2020).
[20] J. Wen, S. Li, Tools for evaluating fault detection and diagnostic methods for Air-Handling Units ASHRAE 1312-RP, 2010.
[21] J. Granderson, G. Lin, R. Singla, E. Mayhorn, P. Ehrlich, D. Vrabie, Commercial Fault Detection and Diagnostics Tools: What They Offer, How They Differ, and What's Still Needed, Lawrence Berkeley National Laboratory Recent Work, 1-12, (2018). Available online: https://doi.org/10.20357/B7V88H (accessed on 1 August 2022).
[22] J. Granderson, G. Lin, A. Harding, P. Im, Y. Chen, Building Fault Detection Data to Aid Diagnostic Algorithm Creation and Performance Testing. Sci. Data 7 (2020) 1-14. Available online: https://www.nature.com/articles/s41597-020-0398-6.pdf (accessed on 1 August 2022).
[23] R. Liu, X. Zhou, R. Milbrandt, Experimental Study of Lab Controlled Faults in Dual-Duct VAV System, ASHRAE Transactions, Atlanta, 121 (2015).
[24] A. Rosato, F. Guarino, V. Filomena, S. Sibilio, L. Maffei, Experimental calibration and validation of a simulation model for fault detection of HVAC systems and application to a case study, Energies 13 (2020).

[25] A. Rosato, F. Guarino, S. Sibilio, E. Entchev, M. Masullo, L. Maffei, Healthy and faulty experimental performance of a typical HVAC system under Italian climatic conditions: Artificial neural network-based model and fault impact assessment, Energies 14 (2021).
[26] A. Rosato, F. Guarino, M. Youssef, S. Sibilio, L. Maffei, Preliminary symptoms assessment of typical faults related to the fans and humidifiers of HVAC systems based on experimental data collected during Italian summer and winter, IOP Conference Series: Earth and Environmental Science 897 (2021).
[27] B. Wu, W. Cai, F. Cheng, H. Chen, Simultaneous-fault diagnosis considering time series with a deep learning transformer architecture for air handling units, Energy & Buildings 257 (2022).
[28] H. Liao, W. Cai, F. Cheng, S. Dubey, P.B. Rajesh, An Online Data-Driven Fault Diagnosis Method for Air Handling Units by Rule and Convolutional Neural Networks, Sensors 21 (2021) 4358.
[29] HVAC SIMulation PLUS other systems (HVACSIM+). Available online: https://www.nist.gov/services-resources/software/hvac-simulation-plus-other-systems-hvacsim (accessed on 1 August 2022).
[30] A. Casillas, G. Lin, J. Granderson, Curation of Ground-Truth Validated Benchmarking Datasets for Fault Detection & Diagnostics Tools; Lawrence Berkeley National Laboratory: Berkeley, CA, U.S.A., 2021. Available online: https://eta-publications.lbl.gov/sites/default/files/curation_of_ground-truth_validated_benchmarking_datasets_for_fault_detection_acasillas_0.pdf (accessed on 1 August 2022).
[31] R.I. Hu, J. Granderson, D.M. Auslader, A. Agogino, Design of machine learning models with domain experts for automated sensor selection for energy fault detection. Appl. Energy 235 (2019) 117-128.
[32] Y. Chen, G. Lin, Z. Chen, J. Wen, J. Granderson, A simulation-based evaluation of fan coil unit fault effects, Energy and Buildings, 263 (2022) 112041.
[33] R. Zhang, T. Hong, Modeling of HVAC operational faults in building performance simulation, Applied Energy 202 (2017) 178-188.
[34] Y. Li, Z. O'Neill, A critical review of fault modeling of HVAC systems in buildings, Build. Simul. 11 (2018) 953-975.
[35] H.H. Hosamo, P.R. Svennevig, K. Svidt, D. Han, H.K. Nielsen, A Digital Twin Predictive Maintenance Framework of Air Handling Units based on Automatic Fault Detection and Diagnostics, Energy Build. (2022) 111988
[36] Y. Li, Z. O'Neill, A critical review of fault modeling of HVAC systems in buildings, Build. Simul. 11 (2018) 953-975.
[37] A. Montazeri, S.M. Kargar, Fault detection and diagnosis in air handling using data-driven methods, Journal of Building Engineering, 31 (2020) 101388.
[38] S.H. Cho, Y.J. Hong, W.T. Kim, M. Zaheer-uddin, Multi-fault detection and diagnosis of HVAC systems:an experimental study, Int. J. Energy Res. 29 (2005) 471-483.
[39] D. Dey, B. Dong; Z. Li, A Probabilistic Framework To Diagnose Faults in Air Handling Units, In Proceedings of the International High Performance Buildings Conference, Purdue University, U.S.A., 2016. Available online: http://docs.lib.purdue.edu/ihpbc/168 (accessed on 9 September 2022).
[40] S.H. Cho, H.C. Yang, M. Zaheer-uddin, B.C. Ahn, Transient pattern analysis for fault detection and diagnosis of HVAC systems, Energy Conversion and Management 46 (2005) 3103-3116.
[41] B. Feng, Q. Zhou, J. Xing, Q. Yang, X. Qin, Y. Mo, W. Chen, A fully distributed voting strategy for AHU fault detection and diagnosis based on a decentralized structure, Energy Reports 8 (2022) 390-404.
[42] O. Nehasil, L. Dobiášová, V. Mazanec, J. Široky. (2021) "Versatile AHU fault detection - Design, field validation and practical application." Energy & Buildings 237 (2021) 110781-110792.
[43] SENS i-Lab, Department of Architecture and Industrial Design, University of Campania Luigi Vanvitelli. Available online: https://www.architettura.unicampania.it/images/ricerca/laboratori/EN/SENS-i_Lab_2021_EN.pdf (accessed on 1 August 2022).
[44] CAREL, Humidifiers Technical Datasheet. Available online: https://www.carel.com/documents/10191/0/%2B030220621/92fca658-a251-49ee-9979-b8829fcba49f?version=1.0 (accessed on 1 August 2022).
[45] AERMEC, Reversible Air/Water Heat Pump Technical Datasheet. Available online: https://download.aermec.com/docs/schede/ANL-021-203-HP_Y_UN50_03.pdf?r=14395 (accessed on 1 August 2022).

[46] R. Mastrullo, A. Rosato, G.P. Vanoli, J.R. Thome, A methodology to select the experimental plant instrumentation based on an a priori analysis of measurement errors and instrumentation cost, International Communications in Heat and Mass Transfer 35 (2008) 689-695.
[47] SIEMENS, Duct Sensors Technical Datasheet. Available online: https://www.downloads.siemens.com/download-center/Download.aspx?pos=download&fct=getasset&id1=24897 (accessed on 1 August 2022).
[48] E+E Elektronic, EE210 Outdoor Datasheet. Available online: https://www.epluse.com/fileadmin/data/product/ee210/datasheet_EE210_Outdoor.pdf (accessed on 1 August 2022). (accessed on 1 1 August 2022).
[49] TSI, Q-TRAK Technical Datasheet. Available online: https://tsi.com/getmedia/d2a8d1d1-7551-47fe-8a0f-3c14b09b494b/7575_QTrak_A4_UK_5001356-web?ext=.pdf (accessed on 1 August 2022).
[50] MEASUREIT, Sensors. Available online: https://shop.measureit.eu/sensori.html (accessed on 1 August 2022).
[51] BELIMO, Energy Valve Technical Datasheet. Available online: https://www.belimoseoul.com/data/medium/9d020b80b518dcf144d3cc8db59f777e.pdf (accessed on 1 August 2022).
[52] Y. Yan, J. Cai, Y. Tang, Y. Yu, A Decentralized Boltzmann-machine-based fault diagnosis method for sensors of Air Handling Units in HVACs, Journal of Building Engineering 50 (2022).